AMERICAN SOCIETY FOR MICROBIOLOGY | mBio®

RESEARCH ARTICLE

A Variant Allele in Varicella-Zoster Virus Glycoprotein B Selected during Production of the Varicella Vaccine Contributes to Its Attenuation

Tomohiko Sadaoka,[a,b] Daniel P. Depledge,[c,d,e] Labchan Rajbhandari,[f] Judith Breuer,[g] Arun Venkatesan,[f] Jeffrey I. Cohen[b]

[a]Division of Clinical Virology, Center for Infectious Diseases, Kobe University Graduate School of Medicine, Kobe, Japan
[b]Medical Virology Section, Laboratory of Infectious Diseases, National Institute of Allergy and Infectious Diseases, National Institutes of Health, Bethesda, Maryland, USA
[c]Department of Microbiology, New York University School of Medicine, New York, USA
[d]Institute for Virology, Hannover Medical School, Hannover, Germany
[e]German Center for Infection Research (DZIF), partner site Hannover-Braunschweig, Hannover, Germany
[f]Division of Neuroimmunology and Neuroinfectious Diseases, Department of Neurology, Johns Hopkins University School of Medicine, Baltimore, Maryland, USA
[g]MRC Centre for Medical Molecular Virology, Division of Infection and Immunity, University College London, London, United Kingdom

ABSTRACT Attenuation of the live varicella Oka vaccine (vOka) has been attributed to mutations in the genome acquired during cell culture passage of pOka (parent strain); however, the precise mechanisms of attenuation remain unknown. Comparative sequence analyses of several vaccine batches showed that over 100 single-nucleotide polymorphisms (SNPs) are conserved across all vaccine batches; 6 SNPs are nearly fixed, suggesting that these SNPs are responsible for attenuation. By contrast, prior analysis of chimeric vOka and pOka recombinants indicates that loci other than these six SNPs contribute to attenuation. Here, we report that pOka consists of a heterogenous population of virus sequences with two nearly equally represented bases, guanine (G) or adenine (A), at nucleotide 2096 of the ORF31 coding sequence, which encodes glycoprotein B (gB) resulting in arginine (R) or glutamine (Q), respectively, at amino acid 699 of gB. By contrast, 2096A/699Q is dominant in vOka (>99.98%). gB699Q/gH/gL showed significantly less fusion activity than gB699R/gH/gL in a cell-based fusion assay. Recombinant pOka with gB669Q (rpOka_gB699Q) had a similar growth phenotype as vOka during lytic infection in cell culture including human primary skin cells; however, rpOka_gB699R showed a growth phenotype similar to pOka. rpOka_gB699R entered neurons from axonal terminals more efficiently than rpOka_gB699Q in the presence of cell membrane-derived vesicles containing gB. Strikingly, when a mixture of pOka with both alleles equally represented was used to infect human neurons from axon terminals, pOka with gB699R was dominant for virus entry. These results identify a variant allele in gB that contributes to attenuation of vOka.

IMPORTANCE The live-attenuated varicella vaccine has reduced the burden of chickenpox. Despite its development in 1974, the molecular basis for its attenuation is still not well understood. Since the live-attenuated varicella vaccine is the only licensed human herpesvirus vaccine that prevents primary disease, it is important to understand the mechanism for its attenuation. Here we identify that a variant allele in glycoprotein B (gB) selected during generation of the varicella vaccine contributes to its attenuation. This variant is impaired for fusion, virus entry into neurons from nerve terminals, and replication in human skin cells. Identification of a variant allele in gB, one of the essential herpesvirus core genes, that contributes to its attenuation may provide insights that assist in the development of other herpesvirus vaccines.

KEYWORDS attenuation mechanism, glycoprotein B, live attenuated varicella vaccine, varicella-zoster virus, virus fusogen

Invited Editor Anthony L. Cunningham, Westmead Institute for Medical Research

Editor Kanta Subbarao, The Peter Doherty Institute for Infection and Immunity

Address correspondence to Tomohiko Sadaoka, tomsada@crystal.kobe-u.ac.jp.

The authors declare no conflict of interest.

Received 30 June 2022
Accepted 13 July 2022
Published 2 August 2022

The live-attenuated varicella-zoster virus (VZV) vaccine Oka strain (vOka) is the first and only licensed vaccine to protect against varicella. The vaccine was developed by serial passage of the parental Oka strain (pOka) in human embryonic lung cells, guinea pig embryo fibroblasts (GPEFs), and human fibroblasts (1). Adaptation of the virus to growth in GPEFs is thought to be primarily responsible for its attenuation in humans. While the vaccine is well tolerated and effectively reduces the burden of varicella (2), vOka establishes latency and can reactivate in otherwise healthy individuals, albeit to a significantly lesser extent than wild-type VZV (3). However, herpes zoster (HZ) associated with vOka can be indistinguishable from wild-type VZV in healthy or in immunocompromised individuals (4–7). In very rare cases, the vaccine has caused fatal disease in severely immunocompromised persons (8, 9). While an adjuvanted recombinant zoster vaccine (RZV) is licensed to prevent HZ and is more effective than the live-attenuated zoster vaccine (10, 11), RZV has not been tested to prevent varicella. Studies of RZV suggest that priming by natural infection or administration of the live-attenuated vaccine may be essential for the ability of RZV to recall VZV-specific T-cell immunity (12, 13), which is considered to be the correlate of protection to prevent HZ (14–16).

Due to the lack of a small animal model that results in varicella, the mechanisms of attenuation of vOka are poorly understood (17). Recent advances in sequencing technology have been informative for analysis of virus variants in vaccine preparations and in humans. During production of vOka by cell culture, multiple single nucleotide polymorphisms (SNPs) accumulated in multiple viral genomes (18) and the sequence of vOka is highly heterogenous with 150 to 466 SNPs in the three available commercial vOka preparations (19–21). Of these SNPs, 137 are consistently observed across the different preparations and are defined as core SNPs. Six of the core SNPs are near fixation ($>$ 90%) in all the preparations indicating that these six core SNPs (five of the six are in ORF62 and the other in ORF0) are highly likely to be responsible for attenuation of vOka (19). Strikingly, another live-attenuated vaccine, strain SuduVax, shares all six core SNPs reinforcing the contributions of the six core SNPs in attenuation of vOka (22, 23). However, pOka/vOka recombinants generated using cosmids or other mutant viruses produced using bacterial artificial chromosome (BAC) systems have not identified a relationship between these six core SNPs and attenuation of vOka (24, 25).

We hypothesized that the discrepancy between the comparative genomics and mutagenesis approaches regarding the role of SNPs in attenuation of vOka may be due to the lack of information about the population diversity within the original pOka isolate. Originally, SNPs in vOka were identified by comparing sequences with pOka obtained by traditional Sanger sequencing, an inefficient method for identifying heterogenous populations of viruses in which two or more alleles are present. Therefore, we reanalyzed the population diversity of pOka using data we previously obtained by Illumina deep sequencing in combination with targeted enrichment technology (21).

RESULTS

A SNP at nucleotide position 2096 in ORF31, encoding glycoprotein B, is maintained in heterogenous populations of pOka. We received pOka directly from Dr. Michiaki Takahashi at passage 6 following the original virus isolation and passaged the virus three additional times in MRC-5 cells prior to sequencing to generate pOka_P9 (21). Reanalysis of Illumina sequencing data derived from pOka_P9 genomic DNA (21) identified 61 sites, of which 15 are located in the duplicate loci (internal repeat short [IR_S] and terminal repeat region [TR_S]) with variant allele frequencies $>$5% at which variant alleles were present with the pOka reference sequence (pOka_AB097933.1), which was previously generated by Sanger sequencing (18). As the current study focuses on pOka and vOka, we use nucleotide (nt) position numbers based on pOka_AB097933.1 while Dumas__NC001348.1 is simultaneously listed in Table 1 for better comparison with previous genetic analyses of VZV. Of 61 polymorphic sites, 35 sites had 10% or more variant frequencies (either pOka_P9 or pOka_R5; see below) (Table 1). In total, 28 single nucleotide polymorphism (SNPs), 2 insertions of 3 to 4 nt, 3 deletions of 1 nt, 1

TABLE 1 Variant frequencies at SNPs and indels in the pOka genome by Illumina sequencing analysis[a]

ORF	nc	0	4	6	22	nc	31	nc	38	nc	62							
Position (pOka_AB097933.1)	51	177	3555	8531	40407	42273	58777	60130	69711	104973	105378	105517	106227	106444	106509	106901	107217	108261
Nucleotide (nt) in pOka_AB097933.1	a	g	c	t	c	g	a	c	t	c	t	t	t	t	t	a	t	t
nt variant	c	c	t	c	-c	-aa	g	-a / -aa	g	-c	c	c	c	c	c	c	c	c
Amino acid (AA) in pOka_AB097933.1	nc	A	V	K	F/S	nc	Q	nc	S	nc	S	T	R	A	T	V	S	S
AA variant	nc	A	I	E	F/S	nc	R	nc	G	nc	G	T	G	A	A	G	G	G
pOka-P9 nt variant %	11.7	99.9	12.6	0.0	29.8	38.9	48.5	35.1	10.3	30.5	1.1	0.4	23.2	0.2	12.7	10.3	1.1	4.0
pOka_R5 (passaged in MRC5) nt variant %	6.3	99.4	2.3	23.8	29.4	30.9	77.3	33.2	12.4	30.0	80.3	19.7	21.5	22.4	0.8	8.7	53.3	18.0
pOka_W (passaged in MeWo) nt variant %	6.9	99.8	2.9	33.3	30.8	28.0	91.0	29.1	10.0	27.8	92.4	28.3	35.4	44.7	0.8	7.9	68.9	27.5
nt in pOka_JN704698.1	a	c	c	t	c	g	g	c	t	c	t	t	c	t	c	a	t	c
nt in pOkaBAC	a	c	c	c	c	g	g	c	t	c	c	t	c	t	t	a	t	c
nt in pOkaBAC_ORF31_2096A	a	c	c	c	c	g	a	c	t	c	c	t	c	t	t	a	t	c
nt in pOkaBAC_ORF31_2096G	a	c	c	c	c	g	g	c	t	c	c	t	c	t	t	a	t	c
Position (Dumas_NC001348.1)	51	178	3556	8532	40489	42391	58914	60266	69850	105010	105413	105552	106262	106479	106544	106936	107252	108296

ORF	nc			67	nc					71							
Position (pOka_AB097933.1)	109161	109246	112233	114938	117864	117874	119629	120861	120946	121846	122890	123206	123598	123663	123880	124590	124729
Nucleotide (nt) in pOka_AB097933.1	t	t	g	a	a	c	g	a	a	a	a	t	a	a	a	a	a
nt variant	c	g	+aaa / +aaaa	g	+ttt / +tttt	t	-t	c	g	g	g	g	g	g	g	g	g
Amino acid (AA) in pOka_AB097933.1	nc	nc	nc	G	nc	nc	nc	nc	nc	S	S	V	T	A	R	T	S
AA variant	nc	nc	nc	G	nc	nc	nc	nc	nc	G	G	G	A	A	G	T	G
pOka-P9 nt variant %	13.5	26.5	14.9	0.1	17.70	15.80	10.10	25.00	13.10	4.00	0.90	10.30	11.70	0.10	23.40	0.40	1.20
pOka_R5 (passaged in MRC5) nt variant %	15.8	77.9	18.1	25.8	17.50	7.70	6.30	78.10	15.70	17.90	52.70	8.70	1.00	23.90	20.70	18.80	79.10
pOka_W (passaged in MeWo) nt variant %	31.9	55.7	17.7	20.6	17.50	7.10	5.80	57.20	32.00	27.00	68.90	7.90	1.00	43.70	34.50	29.00	92.00
nt in pOka_JN704698.1	t	g	g	a	a	c	g	c	a	g	a	t	g	a	g	a	a
nt in pOkaBAC	t	g	g	a	a	c	g	c	a	g	a	t	a	a	g	a	g
nt in pOkaBAC_ORF31_2096A	t	g	g	a	a	c	g	c	a	g	a	t	a	a	g	a	g
nt in pOkaBAC_ORF31_2096G	t	g	g	a	a	c	g	c	a	g	a	t	a	a	g	a	g
Position (Dumas_NC001348.1)	109196	109281	112127	114833	117759	117770	119527	120616	120701	121601	122645	122961	123353	123418	123635	124345	124484

[a]nc, noncoding; F/S, frameshift; green highlighting, nt variant not previously reported in pOka_AB097933.1; shaded green highlighting, the percentage of the virus population with nt variant.

deletion of 1 to 2 nt, and 1 deletion of 2 nt were identified. Six insertions or deletions (indels) were located in noncoding regions and one deletion at position 40407 in the ORF22 gene caused a frameshift in about 30% of genomes. Of the 28 SNPs, 6 were located within noncoding regions, 6 produced synonymous changes, and 16 produced nonsynonymous changes (highlighted in gray in Table 1).

Variant frequencies for most of the SNPs causing nonsynonymous changes were less than 15%; however, two alleles (guanine [G] or adenine [A]) at nt position 58777 corresponding to nt 2096 in the ORF31 coding sequence were present at nearly equal frequencies in pOka_P9 (51.5% for A and 48.5% for G) (Table 1). The allele, 2096G in the ORF31 gene (ORF31_2096G) was not reported in pOka_AB097933.1 (18) but was described in another pOka genome sequence, pOka_JN704698.1, which did not examine the population diversity within the pOka sample that was used (26). While exact passage numbers of pOka_AB097933.1 were not reported (18), pOka_JN704698.1 was reported to be passaged six times in human embryonic lung fibroblast (HELF) cells after receipt before analysis by 454 sequencing technology (26). ORF31 is one of the core genes conserved in all herpesviruses and encodes glycoprotein B (gB), which functions as a fusogen and is essential for entry of herpesviruses into host cells (27). The 2096G allele results in an arginine at amino acid (aa) position 699 (699R) within domain V of gB (28, 29), while the 2096A allele results in glutamine (699Q). In all the preparations of vOka (OkaVax [Biken], VariRix [GSK], and VariVax/ZostaVax [Merck]) available in 2016, the 2096G allele was never reported (19), whereas only 0.01% of genomes contained 2096G in the live-attenuated zoster vaccine (Zostavax, derived from vOka) previously obtained from Merck (21). Importantly, a pOkaBAC genome, established from virus passaged multiple times in HELF cells, before cloning into a BAC vector (30) contains ORF31_2096G (Table 1). These results demonstrate that an early passage of pOka contained a heterogenous population of viral genomes and suggest that the virus population with ORF31_2096G was eliminated during production of vOka.

pOka with the 2096G allele in ORF31 is selected over the 2096A allele for axonal infection of human embryonic stem cell-derived neurons in a microfluidic device. An *in vitro* VZV latency system using human embryonic stem cell (hESC)-derived neurons in combination with a microfluidic device (21, 31) provided a unique opportunity

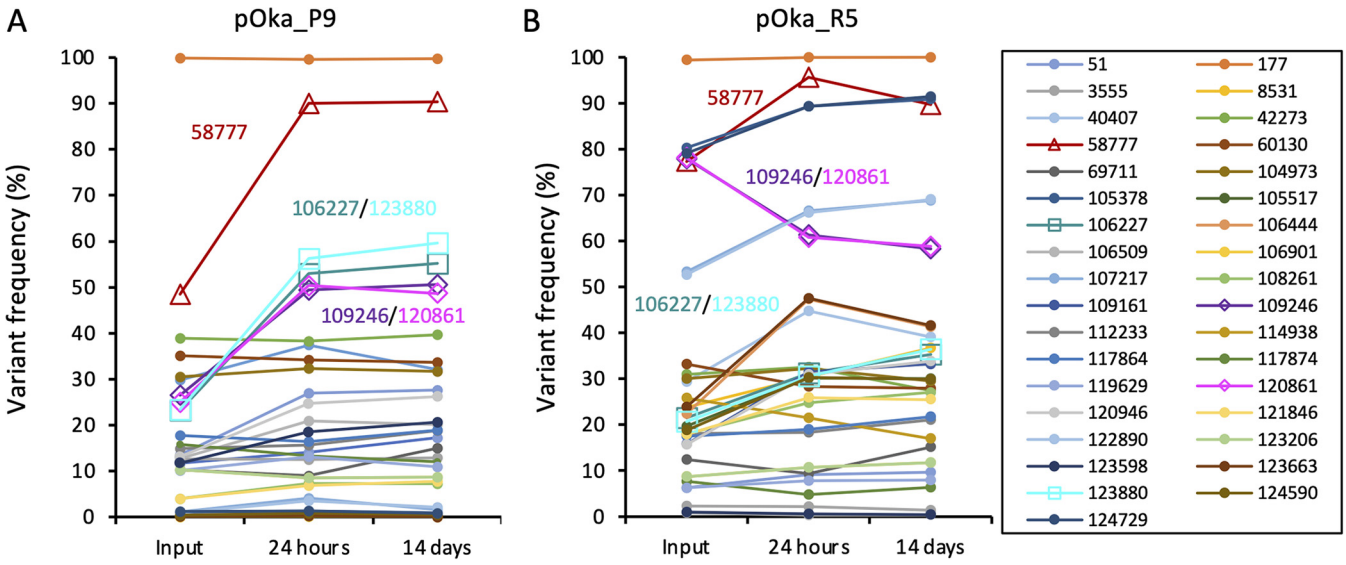

FIG 1 Change in variant frequency of SNPs in pOka before and after axonal infection of human neurons. The percent of the frequency of variants of all the SNPs in pOka_P9 (A) and pOka_R5 (B) before axonal infection (input), at 24 h after infection (A) and mean of biological triplicates (B), and 14 days after infection (mean of biological triplicates [A] and quadruplicates [B]) are shown with nucleotide position based on pOka_AB097933.1 (see Table 1).

to analyze viral entry from peripheral axon termini. hESC-derived neurons are highly permissive for VZV lytic infection by direct infection of the neuronal soma (cell body) either using cell-free or cell-associated virus (32) or by axonal infection of cell-associated virus (33); however, VZV infection of axon terminals with cell-free virus in this system results in viral genome transfer to the neuronal soma and establishment of latency (21, 31, 34).

Axonal infection with pOka_P9 cell-free virus, which contained similar frequencies of A (51.5%) and G (48.5%) at nt 2096 of ORF31, followed by Illumina sequencing of viral genomes isolated from neuronal soma at 14 days postinfection (dpi) showed that the 2096G allele increased from 48.5% (input) to 90.4 ± 0.47% (mean ± SEM [standard error of the mean] of three biological replicates) (Fig. 1A, position 58777 labeled in red triangle) (21). Consistent with the increased variant frequency of 2096G at 14 dpi by the axonal route, 90.0% of the pOka genomes in neuronal soma at 24 h postinfection (hpi) by the axonal route had the 2096G allele in ORF31. Other than the SNP at nt 2096 in ORF31, the only other alleles that had an appreciable change in frequency after axonal infection were the 2872G allele in ORF62/ORF71 (duplicate gene), which increased from 23.2/23.4% to 53.0/56.3% at 24 hpi and was maintained at 55.2 ± 0.35/59.6 ± 2.42% at 14 dpi (Fig. 1A, 106227/123880 labeled in teal/cyan square), and the 109246/120861G allele in the noncoding region between ORF62 and ORF63 (duplicate loci), which increased from 26.5/25.0% to 49.4/50.4% at 24 hpi and was maintained at 50.6 ± 0.76/48.7 ± 1.19% at 14 dpi (Fig. 1A, 109246/120861 labeled in violet/magenta diamond).

In addition to pOka_P9, pOka_R5 passaged in HELF and MRC-5 cells (<10 times) was also examined. pOka_R5 had 77.3% of ORF31 with the_2096G allele (Table 1). Axonal infection of the pOka_R5 resulted in enrichment of ORF31_2096G from 77.3% to 95.6 ± 2.60% at 24 hpi (three biological replicates) and 89.7 ± 2.89% at 14 dpi (four biological replicates) (Fig. 1B, 58777 labeled in red triangle). An increase of ORF62/71_2872G from 21.5/20.7% to 31.2 ± 2.30/30.6 ± 2.16% (24 hpi) and 35.3 ± 1.95/36.4 ± 1.33% (14 dpi) was also observed (Fig. 1B, 106227/123880 labeled in teal/cyan square), whereas the 109246/120861G in the noncoding region between ORF62 and ORF63 was decreased from 77.9/78.1% to 61.3 ± 3.60/60.8 ± 3.90% (24 hpi) and 58.3 ± 0.49/58.9 ± 0.78% (14 dpi) (Fig. 1B, 109246/120861 labeled in violet/magenta diamond). Because neither viral replication nor production of infectious progeny virus is observed in this system up to 70 dpi in the absence of reactivation stimuli (21), the consistent selection of the 2096G allele in ORF31 encoding gB indicates that pOka with

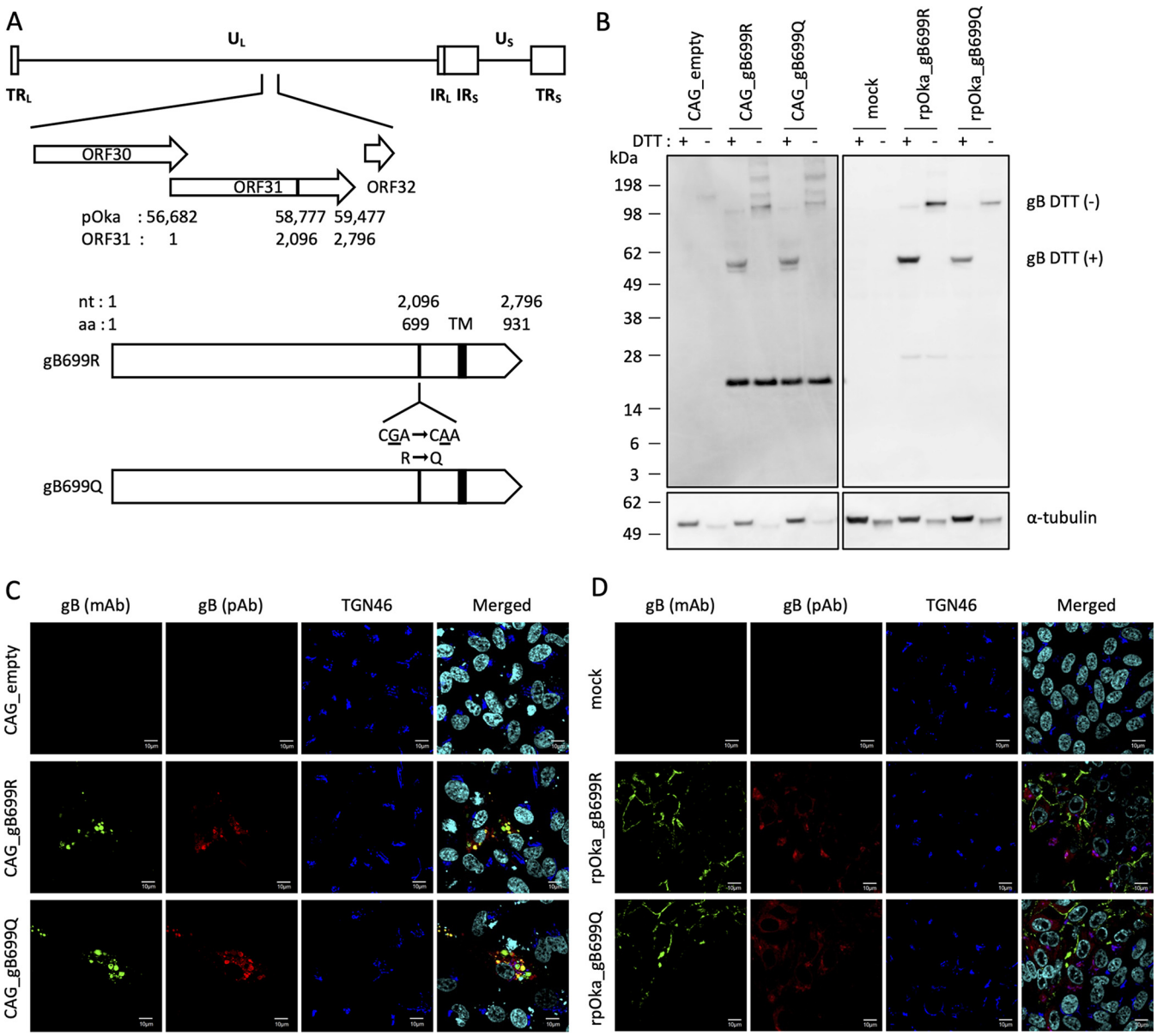

FIG 2 Characterization of gB699R and gB699Q expressed by plasmid transfection or by VZV infection. (A) Location of ORF31 in VZV genome (nucleotide numbering based on pOka_AB097933.1), location of the ORF31 SNP 2096G/2096A with corresponding nonsynonymous aa change in ORF31/gB (bottom). U_L, unique long; U_S, unique short; TR_L, terminal repeat long; IR_L, internal repeat long; IR_S, internal repeat short; TR_S, terminal repeat short; TM, transmembrane region. (B) Immunoblotting analysis of gB699R and gB699Q by transfection (left) and infection (right) in ARPE-19 cells using anti-gB polyclonal antibody and anti-α-tubulin MAb as internal control. DTT, dithiothreitol. Molecular mass standards (kDa) are shown at left. (C and D) Confocal microscopic analysis of gB699R and gB699Q localization by transfection (C) and infection (D) in ARPE-19 cells using anti-gB MAb and anti-gB polyclonal antibody along with anti-TGN46 polyclonal antibody. Nuclei were stained with DAPI. Images are representative of results from two independent experiments. Transfection efficiency of ARPE-19 cells was about 40% (B and C). Magnification; $\times$600 and $\times$2 digital zoom with 10 μm of white bars.

gB 699R (2096G) is dominant over gB 699Q (2096A) in a mixed population of viruses for entry into axon termini of hESC-derived neurons.

The amino acid difference at 699 of gB does not affect the level of gB when expressed alone or in the context of VZV lytic infection. To test whether the SNP at position 2096 in ORF31 affects levels of gB, human retinal pigmented epithelial (ARPE-19) cells, which support VZV lytic infection, were either transfected with plasmid CAG_gB699R or CAG_gB699Q (which express gB with an R or G at aa 699, respectively) or infected with recombinant pOka virus with gB699R (rpOka_gB699R) or gB699Q (rpOka_gB699Q) (Fig. 2A). VZV gB is cleaved into two portions by the cellular furin protease or other subtilisin-like pro-protein convertases via an RSRR motif located at aa positions 491 to 494 of gB

and generates a heterodimer consisting of the N-terminal (494 aa) and C-terminal (437 aa) portions of the glycoprotein held together by disulfide bonds (35). Transfection of cells with plasmids CAG_gB699R or CAG_gB699Q resulted in equal levels of gB whether the cell lysates were treated with dithiothreitol (DTT) (yielding the two cleavage products of gB; only the C-terminal portion is recognized by anti-gB polyclonal antibody) or not treated with DTT (showing the heterodimeric form of gB) (Fig. 2B, left). A dominant band of 20 kDa was detected with anti-gB polyclonal antibody in ARPE-19 cells transfected with the plasmid expressing gB699R/Q, but not in cells transfected with empty vector, regardless of whether or not the cell lysates were treated with DTT. A 20-kDa band was also observed in membrane protein-enriched extracellular vesicles containing gB produced in HEK-293T cells using the anti-gB antibody (see below), and a 26-kDa band was seen in ARPE-19 cells after infection with VZV (see below). We speculate that these bands are caused by further cleavage of the C-terminal portion of gB as the antibody recognizes the C terminus of gB. The variability of detection of α-tubulin, used as a loading control for the samples treated with and without DTT, indicates that recognition of the anti-α-tubulin antibody is weaker in the absence of DTT (Fig. 2B, bottom). Confocal microscopy did not show any differences in cellular localization between gB699R and gB699Q; both variants formed cytoplasmic vesicle-like structures but rarely colocalized with *trans*-Golgi network (TGN) if expressed in the absence of VZV infection (Fig. 2C). In the context of VZV infection, there was again no difference between gB699R and gB699Q either in the size in the presence or absence of DTT (Fig. 2B, right) or in the cellular localization both at the cell surface or with the TGN (Fig. 2D). Thus, gB expression, cleavage, heterodimer formation, and localization were not affected by the difference at amino acid position 699 of gB.

rpOka_gB699Q shows a similar phenotype to vOka, while rpOka_gB699R resembles pOka for cell-to-cell spread during lytic infection in cell culture. To test whether the allele selection at position 2096 of ORF31 of vOka contributes to its attenuation during lytic replication in cell culture and spread between cells, different cell lines were infected with pOka (pOka_R5), rpOka_gB699R, rpOka_gB699Q, or vOka. Cell-free virus inocula were prepared in and titrated in MRC-5 cells, which are used for production of vOka vaccine, and the same titer of each virus was used for viral growth assays.

In MRC-5 cells, no significant differences were observed in size of infectious foci or virus replication among all the various viruses tested (Fig. 3A and B). By contrast, in ARPE-19 cells rpOka_gB699Q formed foci comparable in size to those observed with vOka but significantly smaller foci than those seen with rpOka_gB699R (Fig. 3C) despite similar levels of replication of all the viruses (Fig. 3D). In MeWo cells, like ARPE-19 cells, the size of infectious foci of rpOka_gB699Q was comparable with those observed with vOka but significantly smaller than those with rpOka_gB699R (Fig. 3E). Despite the use of the same amount of cell-free virus, based on virus titrations performed in MRC-5 cells, vOka and rpOka_gB699Q produced fewer infectious foci than rpOka_gB699R and pOka in MeWo cells throughout infection; however, the growth curve pattern of all the viruses was parallel, indicating that once lytic infection is established in MeWo cells, levels of replication of vOka and rpOka_gB699Q in MeWo cells were nearly identical to rpOka_gB699R and pOka (Fig. 3F). This is consistent with the previously reported identical growth curves of wild-type VZVs and vOka in MeWo cells (24, 36). Taken together, rpOka_gB699Q was indistinguishable from vOka for virus replication, and both viruses show reduced cell-to-cell spread in ARPE-19 cells and MeWo cells compared with pOka and rpOka_gB699R.

Amino acid 699 of VZV gB is important for its fusion activity. Since VZV gB is part of the core fusion machinery along with gH/gL (37, 38), we compared the fusion activity of gB699R/gH/gL with gB699Q/gH/gL in a luciferase-based VZV glycoprotein-mediated cell fusion assay. Consistent with the results of transient expression of gB699R and gB699Q in ARPE-19 cells (Fig. 2), total cell levels (Fig. 4A) and cellular localization (Fig. 4B) of gB699R and gB699Q were comparable in HEK-293T cells. Cell surface levels of gB699R and gB699Q were also similar in transfected HEK-293T cells (Fig. 4C). When coexpressed with gH/gL, total cell levels, cellular localization, and cell surface

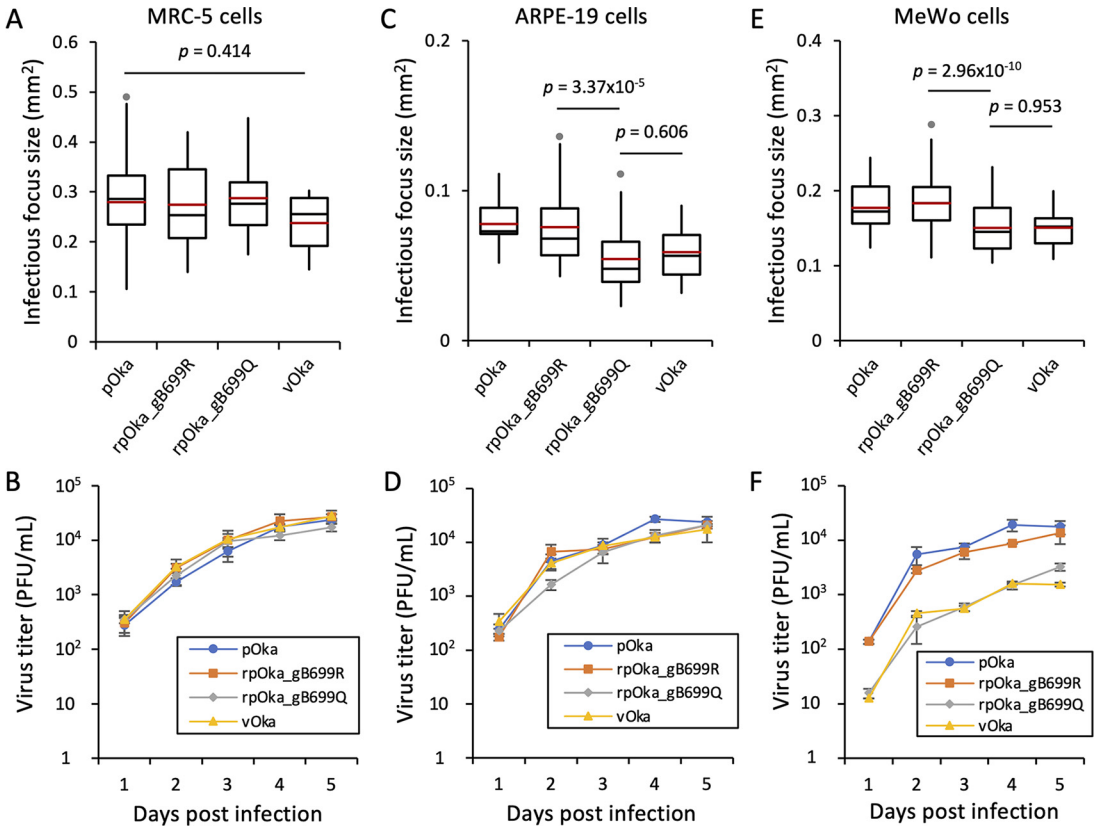

FIG 3 Comparison of phenotype of VZV with different gB SNPs in different cell types. Infectious focus size (A, C, and E) and virus growth (B, D, and F) were compared in MRC-5 (A and B), ARPE-19 (C and D), and MeWo (E and F) cells. Representative data from two independent experiments is shown for each analysis. Infectious focus size is shown in Box and Whisker plots using the Tukey method (n = 30 to 50 foci) measured in each cell type. Red line, mean; gray circle, outliers. P value was calculated by one-way ANOVA with Fisher's least significant difference (LSD) correction for multiple comparisons. Each virus titer is shown as a mean (symbol) with standard error of the mean (SEM; bar) of replicates.

levels of gB699R and gB699Q were similar (Fig. 4A and B, and 4C, respectively). Coexpression of gB with gH/gL reduced total and cell surface levels of gB compared with expression of gB alone (Fig. 4A and C).

gB699R/gH/gL showed significantly higher fusion activity than gB699Q/gH/gL at 48 h after mixing ARPE-19 target cells expressing T7 polymerase with HEK-293T cells expressing gH/gL, gB, and luciferase driven by the T7 promoter (P = 0.00003, Fig. 4D). However, gB699R/gH/gL and gB699Q/gH/gL showed similar levels of fusion activity when fusion was measured at 24 h after cell mixing (P = 0.35134, Fig. 4D). Fusion activity of gB699R/gH/gL was significantly higher than gB699Q/gH/gL at both 24 and 48 h after mixing when MeWo cells were used as target cells instead of ARPE-19 cells (P = 0.00003 or P = 0.00007, respectively; Fig. 4D). Fusion activity was negligible when either ARPE-19 or MeWo target cells expressing T7 polymerase were mixed with HEK-293T cells expressing luciferase driven by the T7 promoter and gB699R or gB699Q without gH/gL or gH/gL without gB (Fig. 4D). Taken together, we found that both gB699R and gB699Q induce membrane fusion along with gH/gL; however, a single amino acid substitution (R to Q) at position 699 in gB significantly reduced glycoprotein-mediated membrane fusion activity for gB/gH/gL.

Membrane protein-enriched extracellular vesicles containing gB reduce axonal infection of neurons with rpOka_gB699Q. To further analyze how the difference in gB sequences affect entry of VZV, we used membrane protein-enriched extracellular vesicles (MPEEVs) (39) to isolate vesicles that could deliver gB699R or gB699Q to cells prior to infection with VZV. MPEEVs contain intact membrane proteins with their correct topology on the surface of virus-like vesicles and have been shown to be useful

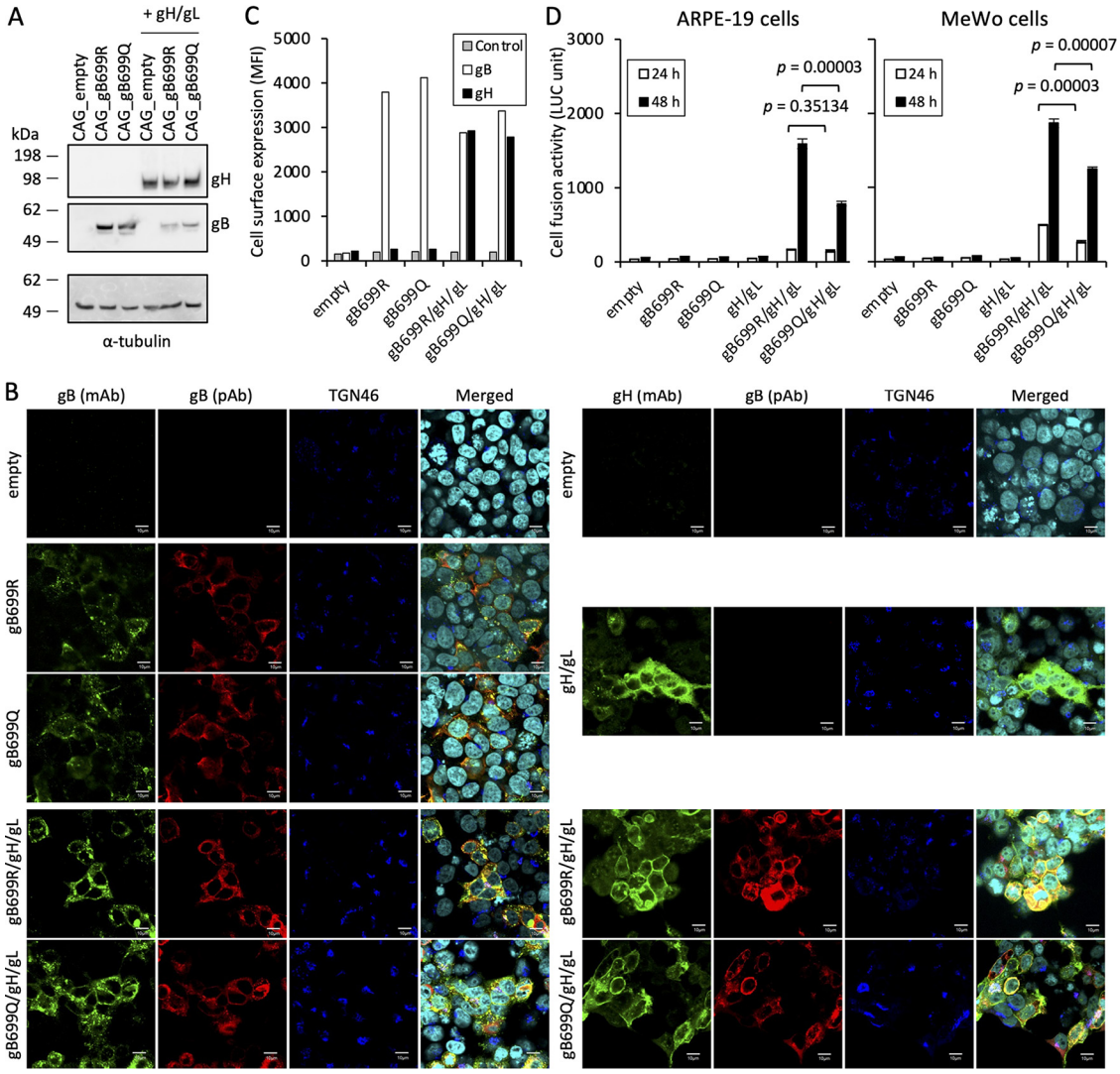

FIG 4 Expression and fusion activity of gB/gH/gL in a cell-based quantitative fusion assay. Total protein expression (A), cellular localization (B), and cell surface expression (C) of gB and gB/gH/gL were compared in HEK-293T cells used as effector cells for the cell-based fusion assay. (A) Immunoblotting by anti-gB polyclonal antibody, anti-gH Mab, and anti-α-tubulin MAb in the presence of DTT (dithiothreitol). Molecular mass standards (kDa) are shown at left. (B) Confocal microscopic analysis using anti-gB polyclonal antibody and anti-gB MAb or anti-gH MAb along with anti-TGN46 polyclonal antibody. Nuclei were stained with DAPI. Magnification is $\times$600 and $\times$2 digital zoom; white bars represent = 10 μm. (C) Flow cytometry using anti-gB MAb or anti-gH MAb. Anti-ORF62 MAb was used as a negative control. Cell surface expression level is shown by mean fluorescent intensity (MFI) obtained from 50,000 events. (A to C) Representative data from two independent experiments is shown for each analysis. (D) Quantitative luciferase-based cell-to-cell fusion assay. Effector HEK-293T cells expressing VZV glycoprotein(s) with firefly luciferase under the control of the T7 promoter, and target ARPE-19 cells (left) or target MeWo cells (right) expressing T7 RNA polymerase were coincubated for the indicated time and luciferase activity (LUC units) was recorded as a measure of cell-to-cell fusion activity. Representative data from three independent experiments are shown with mean and SEM (standard error of the mean) of four biological replicates. *P* value was calculated by one-way ANOVA with Fisher's LSD correction. Transfection efficiency of HEK-293T cells by PEImax was more than 80% as shown in panel B. Transfection efficiency in ARPE-19 cells by nucleofection was 70 to 80% by FACS using pCAG_EGFP plasmid.

for studying herpes simplex virus 1 (HSV-1) gB (40). We transfected HEK-293T cells with CAG_gB plasmids to maximize their expression and purified MPEEVs expressing gB from cell culture supernatants. gB on purified MPEEV_gB699R or MPEEV_gB699Q was shown to be cleaved and only the C-terminal portion was detected by anti-gB polyclonal antibody in the presence of DTT (Fig. 5A, left, DTT [+]). In the absence of DTT, gB formed a heterodimer through disulfide bonding (Fig. 5A, left, DTT [−]) similar to the gB forms observed in rpOka_gB699R or rpOka_gB699Q cell-free virus (Fig. 5A, middle). VZV gB MPEEVs were readily purified, similar to those reported for HSV-1 gB; by

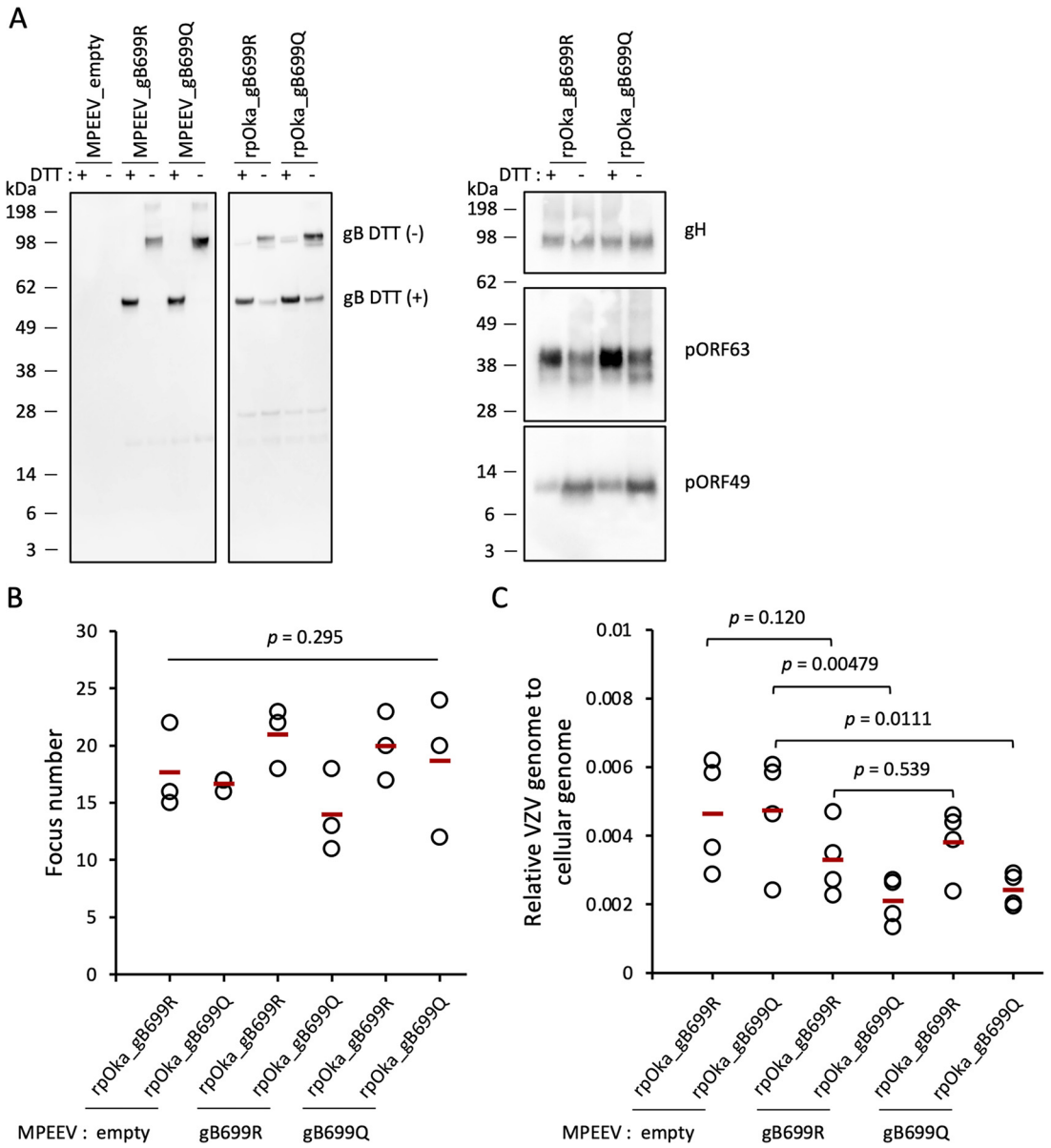

FIG 5 Reduction of infection by membrane protein enriched extracellular vesicles (MPEEVs) expressing gB. (A) Comparison of gB699R and gB699Q from MPEEVs expressing gB (left) and rpOka cell-free viruses (middle) by immunoblotting using anti-gB polyclonal antibody. Other virion components were compared between rpOka_gB699R and rpOka_gB699Q by immunoblotting using anti-gH MAb, anti-pORF63 polyclonal antibody and anti-pORF49 polyclonal antibody (right). DTT, dithiothreitol. Molecular mass standards (kDa) are shown at left. Image is representative of results from three independent experiments. (B) Number of infectious foci generated by each virus after infection in the presence of MPEEVs expressing gB or MPEEV-empty in APRE-19 cells is shown. Biological triplicate data is shown with the mean (red line). *P* value was calculated by one-way ANOVA with Fisher's LSD correction for multiple comparisons. (C) Relative numbers of viral genomes transported to neuronal soma after axonal virus infection in the presence of MPEEV expressing gB or MPEEV-empty are compared between rpOka_gB699R and rpOka_gB699Q. Four biological replicates data are shown with the mean (red line). *P* values were calculated by one-way ANOVA with Fisher's LSD correction for multiple comparisons.

contrast, when coexpressed with gH/gL in HEK-293T cells, no gB/gH/gL MPEEVs were detected despite apparent expression of the glycoproteins in the cells (Fig. 4A).

To determine whether MPEEVs expressing gB can compete with cell-free VZV for entry into cells, ARPE-19 cells were incubated with MPEEV_empty (i.e., not expressing gB), MPEEV_gB699R, or MPEEV_gB699Q (50 μL/well; 10 μL [5 μg]/lane in Fig. 5A, left) for 30 min at 37°C and then infected with VZV cell-free virus (20 PFU [1.5 to 2.0 $\times$ 10^7 genomes based on quantitative PCR]/well) in the presence of MPEEVs for 1 h at 37°C.

Viruses with equal infectious titer contain comparable level of gB (Fig. 5A, middle) and other virion components, gH, pORF63, and pORF49, whereas their recognition by each antibody were variable between the samples of DTT (+) and DTT (−) (Fig. 5A, right). The cells were then treated with low-pH buffer for 30 s to inactivate virus still on the surface of the cells and cultured for 6 days. Neither MPEEV_gB699R nor MPEEV_gB699Q significantly reduced the infectious focus number when compared to MPEEV_empty-treated ARPE-19 cells infected with either rpOka_gB699R or rpOka_gB699Q (Fig. 5B). Similar results were seen in MeWo cells (T. Sadaoka and J. I. Cohen, unpublished data). Thus, MPEEV_gB699R or MPEEV_gB699Q does not compete with rpOka_gB699Q or rpOka_gB699R for entry into ARPE-19 (or MeWo) cells.

Since gB699R is dominant to gB699Q for pOka infection of terminal axons of neurons (Fig. 1A and B), we measured the ability of MPEEVs expressing gB to inhibit infection of rpOka_gB699R or rpOka_gB699Q at neuronal axons by quantifying viral genomes in neuronal soma at 24 hpi (four replicates performed for per each combination of MPEEVs and rpOka_gBs). rpOka_gB699R and rpOka_gB699Q reached the soma equally well in the presence of MPEEV_empty. While MPEEV_gB699R did not reduce infection of rpOka_gB699R ($P = 0.120$), it significantly reduced infection of rpOka_gB699Q ($P = 0.00479$). Even in the presence of MPEEV_gB699Q, infection of the neuronal soma of rpOka_gB699Q via the axon termini was significantly reduced ($P = 0.0111$), but infection of rpOka_gB699R was not inhibited ($P = 0.539$) (Fig. 5C). In summary, infection of the neuronal soma via the axon termini with rpOk_gB699Q was less efficient compared to rpOka_gB699R only in the presence of MPEEV_gB699R or MPEEV_gB699Q.

Selection of pOka with gB699Q contributes to vOka attenuation in human skin cells. Skin tropism is a key feature in the pathogenesis of VZV (41). Reduced replication of vOka compared with pOka in skin, based on the SCID-hu mouse skin xenograft model, has been proposed as an important factor in attenuation of the vaccine virus (24, 42). Deep sequencing of pOka_W (pOka passaged fewer than 10 times in MeWo cells) resulted in enrichment of 2096G/699R of ORF31/gB from 77.3% (pOka_R5) to 91.0% (pOka_W) (Table 1), suggesting that gB699Q in vOka contributes to attenuation of the virus in human skin.

Human neonatal epidermal keratinocytes (HEKn) were infected with cell-free pOka (pOka_R5), rpOka_gB699R, rpOka_gB699Q, or vOka, and the size of infectious foci was compared (Fig. 6A). HEKn are primary cells and have limited cell divisions. We were able to passage HEKn cells more than 10 times but observed that about 10% of the cells have a fibroblast-like morphology at passage number 6. Therefore, we performed experiments only in HEKn cells that had been passaged three times (HEKn_P3). Unlike MRC-5, ARPE-19, and MeWo cells, HEKn cells are difficult to detach and disperse as single cells, an essential step for a viral growth assay. The cells required about 10 min of treatment with trypsin to detach them, resulting in inactivation of virus on the cell surface; therefore, only infectious focus formation using infection with cell-free virus was compared. This assay measures cell-to-cell spread of virus.

All the VZV isolates gave comparable results in infectious foci assays using HEKn_P3 cells (Fig. 6A). Since rpOka_gB699Q and vOka showed reduced replication in MeWo cells compared with rpOka_gB699R and pOka (Fig. 3E and F), infectious focus formation was compared in normal human skin fibroblasts (Hs68 cells). In Hs68 cells, rpOka_gB699Q and vOka formed comparable infectious foci and significantly smaller foci than those formed by rpOka_gB699R and pOka_R5 (Fig. 6B). These results indicate that gB699Q contributes to vOka attenuation in human skin and suggest that vOka is impaired for replication and/or spreading in skin fibroblasts compared with keratinocytes.

To test this hypothesis, we examined infectious focus formation in HEKn_P6 cells, which, as noted above, are a mixture of cells with keratinocyte and fibroblast-like morphologies. rpOka_gB699Q and vOka formed significantly smaller infectious foci than those formed by rpOka_gB699R and pOka_R5 in HEKn_P6 cells (Fig. 6C). These results were similar to those in Hs68 cells but different from those in HEKn_P3 cells. In addition, all the VZV isolates formed significantly larger infectious foci in HEKn_P6 than in HEKn_P3 cells (Fig. 6D). Thus, an amino acid change at position 699 in gB from R to Q is a determinant

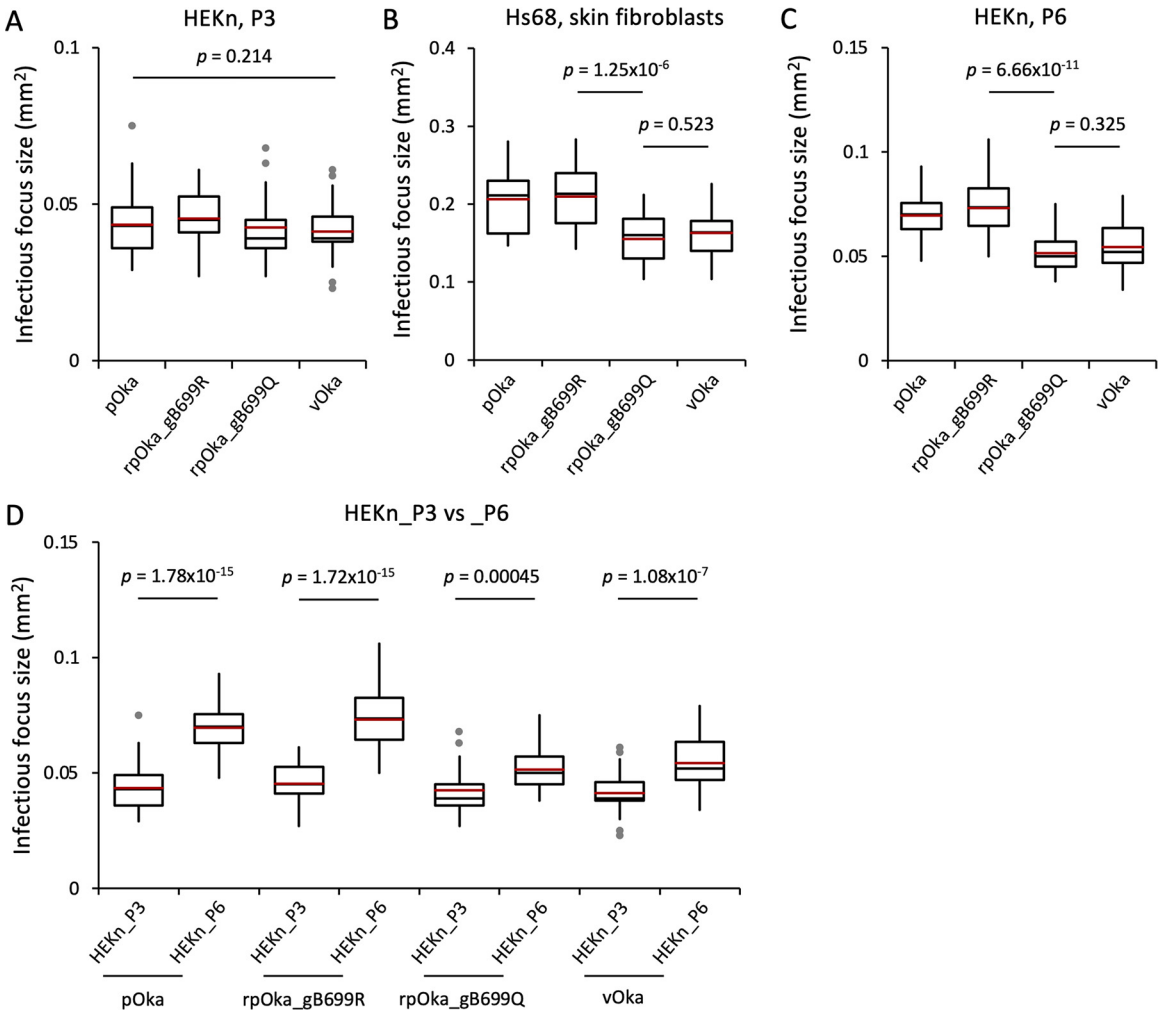

FIG 6 Comparison of the phenotype of VZV with different gB SNPs in human primary skin cells. Infectious focus size after infection of HEKn_P3 cells (A), Hs68 cells (B), and HEKn_P6 cells (C) with different VZV isolates. Infectious focus size after infection of HEKn_P3 and HEK_P6 cells with the same VZV isolate (D). Data were derived from panels A and C. Representative data from two independent experiments are shown for each analysis. Infectious focus size is shown in box and whisker plots using the Tukey method (n = 20 to 50 foci) measured in each cell type. Red line, mean; gray circle, outliers. The P value was calculated by one-way ANOVA with Fisher's LSD correction for multiple comparisons.

for vOka attenuation in human skin, and impaired replication in human skin fibroblasts rather than keratinocytes may contribute to attenuation of vOka.

DISCUSSION

By analyzing the genome sequence heterogeneity of pOka and comparing it with that of vOka, we identified a SNP within the VZV ORF31 gene at which two alleles (G and A) exist at similar frequencies in low passage pOka (pOka_P9) at position 2096; however, one allele, 2096G, was absent in vOka. The SNP located at nt position 2096 (G [absent in vOka] and A [present in vOka]) in the ORF31 gene caused an amino acid change at position 699 (R and Q, respectively) in gB. gB together with gH/gL (37, 38) makes up the core fusion machinery of VZV (43), is essential for VZV entry into cells (44), and is conserved among all herpesviruses (45). The amino acid change at 699 in gB from arginine (R), a basic amino acid, to glutamine (Q), an acidic amino acid, results in reduced fusion activity of gB/gH/gL. rpOka_gB699Q showed a similar phenotype as vOka during lytic infection in cell culture including primary human skin cells, while rpOka_gB699R had a similar phenotype in cells as pOka. When these recombinant viruses were used to infect hESC-derived neurons via axon terminals in a microfluidic

device, both viruses could transfer their genomes equally well to neuronal soma as shown previously for pOka and vOka (21). By contrast, when virus infections were performed in the presence of MPEEVs expressing either gB699R or gB699Q, infection of neurons by rpOka_gB699Q was significantly reduced compared with that of rpOka_gB699R and similar to the reduction of infection of pOka with ORF31_2096A/gB699Q compared with pOka with ORF31_2096G/gB699R. Thus, the current study demonstrates that the presence of the 2096A allele (and absence of the 2096G allele) in ORF31 in vOka is one of the determinants of its attenuation.

The use of nucleotide sequencing has suggested possible mechanisms of attenuation for vOka with the finding of six core SNPs present in ORF62 and ORF0 genes those are nearly fixed in all vOka preparations based on Sanger sequencing or deep sequencing (18–20, 22, 23, 46, 47). However, these studies have all been conducted using sequence information of pOka_AB09733.1, which was obtained by Sanger sequencing with no information on variant alleles present. Thus, the contribution of allele selection at nt position 2096 in ORF31 for attenuation of vOka has not been recognized. Using 454 sequencing, the 2096G allele, but not 2096A, was included in the data set of another pOka genome sequence, pOka_JN704698.1 (26). Analysis of attenuation of vOka by generating chimeric viruses containing portions of pOka and vOka using the cosmid system (48) and analyzing replication of the viruses in human skin xenografts in the SCID-hu mice (49) showed that the ORF30 to 55 loci from the pOka genome were sufficient to maintain the wild-type VZV phenotype in human skin (24). The two chimeric viruses maintaining a pOka phenotype in human skin had either the 2096G or both 2096G and 2096A alleles in their genome (referred as G/A polymorphism at position 58793 in reference 24), while all the other chimeric viruses having a vOka phenotype in human skin had only the 2096A allele. Importantly no other SNP associated with the pOka or vOka phenotype in human skin was reported (24). Our current results using the BAC system based on the comparative genomics of pOka and the previous results using vOka and pOka recombinants by the cosmid system (24) show the importance of the loss of the virus population having the ORF31_2096G/gB699R allele from pOka for attenuation of vOka.

While pOka was isolated in HEL cells at 37°C, it was subsequently passaged 11 times in HEL cells at 34°C and 12 times in GPEFs at 37°C. The resulting virus was further cultured three times in human diploid, WI-38 cells at 37°C and used as vOka (1). It is thought that passage of the virus in guinea pig cells was the key step resulting in its attenuation. SuduVax, another live attenuated VZV vaccine, originally obtained from a VZV isolate in South Korea was isolated in HEL cells and serially passaged 10 times in HEL cells followed by 12 passages in guinea pig embryonic lung fibroblasts and then five passages in HEL cells (22). Adaptation of VZV isolates to guinea pig cells introduced multiple SNPs throughout their genomes, and the allele frequencies at most of these sites vary considerably between vOka and SuduVax (50); however, the six core SNPs are near fixation in both vOka and SuduVax and these SNPs are thought to have a major role for adaptation to growth in guinea pig cells and attenuation in humans. Importantly, SuduVax also has ORF31_2096A as does vOka (50). vOka formed significantly larger infectious foci than pOka in GPEF, and rpOka_gB699Q formed larger foci than rpOka_gB699R in GPEF. However, rpOka_gB699Q showed significantly smaller foci than vOka and foci that were comparable in size to pOka in GPEF (Fig. S1). Since rpOka_gB699Q has a similar attenuation phenotype as vOka in human cells and significantly increased ability for cell-to-cell spread compared to rpOka_gB699R in GPEFs, allele selection of ORF31_2096A/gB699Q might play dual roles in adaptation of vOka to GPEF and its attenuation in human cells. While the data imply that the six core SNPs contribute to vOka adaptation to GPEF, further studies are needed to assess the contribution of the six core SNPs in vOka to attenuation in humans.

Among the six core SNPs, the 106227C allele (known as 106262C in Dumas_NC001348.1 and 2872G in ORF62) has been used to discriminate vOka from wild-type VZV as a "vaccine marker" in samples from patients with varicella or HZ, because nearly 100% of the vOka

population has this allele. Deep sequencing of pOka genomes identified 106227C in pOka (23.2% in pOka_P9, 21.5% in pOka_R5 and 35.4% in pOka_W) and in the pOkaBAC (Table 1). After *in vitro* axonal infection of pOka_P9 or pOka_R5, this "vaccine marker" allele (106227C, ORF62_2872G) in pOka increased along with 58777G (ORF31_2096G). The 106227C allele had no negative impact on rpOka_gB699R in any of the human cells tested. Consistent with this, the six core SNPs, regardless of whether they corresponded to the pOka or vOka SNPs, had no impact on the attenuated phenotype of pOka/vOka chimeric VZVs in a SCID-hu mouse skin xenograft model (24). These results support that the loss of the virus population having the ORF31_2096G/gB699R allele from pOka is a major contributor for attenuation of vOka; further investigation is essential to evaluate the importance of the six core SNPs in vOka attenuation.

In herpesviruses, gB functions as a fusogen (class III) for entry of all herpesviruses into cells. Crystal structures of gB postfusion formed from all herpesvirus subfamilies have been resolved (29, 51–54), and all the homologs adopt similar structures (55) including VZV gB (28). In contrast, the structure of the prefusion form of gB has been reported only for HSV-1 at an overall resolution of 9 Å using a MPEEV-based approach (40, 56, 57). VZV gB 699R/Q is located in domain V of gB comprising a C-terminal arm that packs against a coiled-coil core formed by domain III in the postfusion form. This coil-arm complex is reminiscent of the six-helix bundle, which may provide the energy to drive membrane fusion in class I fusogens (58–60) as proposed for HSV-1 gB (61). gB 699R/Q in VZV corresponds to gB687E in HSV-1 gB, and this glutamic acid is conserved in betaherpesviruses (e.g., human cytomegalovirus [HCMV] strain AD169) and gammaherpesviruses (e.g., Epstein-Barr virus strain B95-8). While the importance of this glutamic acid has not been directly determined in these viruses, mutation of HSV-1 gB at 671I, 681H, or 683F within the C-terminal arm of domain V (corresponding to 683V, 693R, or 695F in VZV, respectively) reduced the ability of HSV-1 gB to execute cell-to-cell fusion (22% to 78% fusion activity compared with wild-type HSV-1) and the combination of all three mutations markedly reduced activity (7% to 9% fusion activity compared to wild-type HSV-1) in a cell-based fusion assay (61). A peptide containing amino acids 678 to 694 of domain V of HCMV gB (corresponding to amino acids 713 to 729 of VZV) inhibited HCMV entry (62), and this effect is postulated to occur by blocking the formation of the postfusion form of gB (54, 59, 63). Similar to HSV-1 or HCMV, a single amino acid change (699R/Q) in domain V of VZV gB causes a significant difference in its fusion activity in a cell-based fusion assay. In addition, rpOka_gB699R and rpOka_gB699Q differ in the size of infectious foci, a measure of cell-to-cell spread due to fusion, when the viruses are grown in ARPE-19 cells, MeWo cells, or human primary skin fibroblasts. Differences in the ability of these two viruses to infect neurons via axon terminals were detected in the presence of MPEEV expressing the two different variants of gB, gB699R/Q. This might be caused by differences in fusion activity of these two viruses as well as other factors including virus entry at axon terminals or intra-axonal transport of virus. A previous study showed that gB is important for spread of HSV-1 from neurons to epithelial cells (64).

Our results using human primary skin cells suggest that vOka attenuation in human skin is mediated by its reduced replication and spread in skin fibroblasts rather than in keratinocytes. The epidermis is the major site for VZV replication in the skin where lesions laden with VZV virions form, although VZV replicates both in the epidermis and dermis (41). Keratinocytes are the main cell type in the epidermis, and several skin infection models have shown a critical role of epidermal keratinocytes for VZV pathogenesis (42, 65–68). However, it is unclear how VZV is transferred from circulating infected T cells during viremia, or from sensory neuronal axons innervating the epidermis and dermis during virus reactivation, to keratinocytes. While keratinocytes comprise nearly 80% of the cells in the epidermis, fibroblasts comprise about 7% of the dermis and a much lesser percentage of the epidermis (69). Our current data, however, suggest that skin fibroblasts might play an important role in VZV pathogenesis as well as in intrinsic skin immunity to VZV.

We have identified that selection of Oka VZV with gB699Q from a heterogenous population of Oka containing gB699R and gB699Q was important to establish attenuated

vOka. One might wonder why gB699Q has been maintained in wild-type circulating VZVs as gB699R should be a virulence factor in human cells and our current data show that passaging of pOka in human cell culture results in enrichment of gB699R. To our surprise, sequencing data of clinical isolates from patients with varicella or HZ do not show ORF31_2096G/gB699R, although most sequenced VZV belongs to clades other than clade 2 to which pOka (and vOka) belong. Only one sequence from a highly passaged Korean clinical isolate from a patient with HZ (KU926318.1) (clade 2) has ORF31_2096G, but its frequency data are not available. Analysis of the population diversity of currently circulating VZVs from multiple clades should provide further information on sequences that are important for virulence, which are common in multiple clades of VZV as well as certain clade-specific sequences.

Taken together, our comparative genomics analyses based on Illumina deep sequencing of pOka and characterization of SNPs combined with our phenotypic studies of the two variant alleles in gB identify a SNP in ORF31 as a novel factor responsible for attenuation of vOka. A more precise understanding of attenuation of vOka would be important not only to improve the safety of the live-attenuated varicella vaccine but might also help in development of live-attenuated vaccines against other human herpesviruses for which no vaccines are currently licensed.

MATERIALS AND METHODS

Cells. Human embryonic stem cell (hESC; H9)-derived neural stem cells (NSC; Thermo Fisher Scientific) were cultured and propagated as described previously (21). For differentiation into neurons, NSCs were used after the third to fifth passages. Neurons were differentiated from NSCs on a microfluidic platform as described previously (21, 70) or with slight modifications using Neurobasal Plus Medium with B-27 Plus Supplement (2% [vol/vol]), GlutaMAX-I (2 mM; Thermo Fisher Scientific), and ascorbic acid (200 μM; Sigma-Aldrich). Human embryonic lung fibroblast MRC-5 cells (JCRB0521, JCRB Cell Bank) were maintained in MEM (minimum essential medium) + GlutaMAX-I (Thermo Fisher Scientific) supplemented with heat-inactivated 8% FBS (fetal bovine serum; Sigma-Aldrich or Biowest). Human retinal pigmented epithelium ARPE-19 cells (CRL-2302; American Type Culture Collection [ATCC]) were maintained in DMEM/F-12 (Dulbecco's modified Eagle medium/nutrient mixture F-12) + GlutaMAX-I (Thermo Fisher Scientific) supplemented with heat-inactivated 8% FBS. Human melanoma MeWo cells (HTB-65, ATCC) and human embryonic kidney (HEK) 293T (CRL-3216; ATCC) cells were cultured in DMEM+GlutaMAX-I (Thermo Fisher Scientific) supplemented with heat-inactivated 8% FBS. Hs68 (IFO50350; JCRB Cell Bank), neonatal normal diploid skin fibroblasts, were cultured and propagated in DMEM+GlutaMAX-I supplemented with heat-inactivated 10% FBS. Human neonatal epidermal keratinocytes, HEKn-APF (Animal Product-Free; Thermo Fisher Scientific), were cultured and propagated in KBM NHEK-XF2 medium (KOHJIN BIO). MeWo_Cre cells expressing Cre recombinase were previously established (71) and cultured in DMEM+GlutaMAX-I supplemented with heat-inactivated 8% FBS. MeWo_T7pol cells expressing T7 RNA polymerase were established by transfecting a DNA fragment containing a puromycin-resistant gene and T7 RNA polymerase expression cassette amplified from pCAG_puro_T7pol plasmid into MeWo cells and selecting in DMEM+GlutaMAX-I supplemented with heat-inactivated 8% FBS and puromycin (0.5 μg/mL; Sigma-Aldrich). Guinea pig embryo fibroblasts (BioWhittaker) were cultured in MEM+GlutaMAX-I supplemented with heat-inactivated 10% FBS.

Viruses. The parental strain VZV Oka (pOka), passage 6 was a generous gift from Michiaki Takahashi (Osaka University), previously described (72) and used at passage 9 from its original isolation yielding pOka_P9. pOka in DCV/CID/KU was maintained in MRC-5 cells (pOka_R5) and additionally passaged in MeWo cells (pOka_W). The vaccine strain VZV Oka (vOka; BIKEN) was propagated in MRC-5 cells. Recombinant pOka (rpOka) viruses, rpOka_gB699R and rpOka_gB699Q, were reconstituted in MRC-5 cells. The BAC cassette within the reconstituted viruses was excised in MeWo_Cre cells. Cell-free virus was prepared from VZV-infected MRC-5 cells by sonication and centrifugation as described previously (72) using an ultrasonic disruptor (UD-100; TOMY Seiko) at an output level 80 for 15 s.

DNA isolation and quantitative PCR. Viral DNA was isolated from VZV-infected cells or cell-free virus using the AllPrep DNA/RNA minikit (Qiagen) or the FavorPrep Blood/Cultured Cell Total RNA minikit (FAVORGEN BIOTECH) in combination with the NucleoSpin RNA/DNA buffer set (Macherey-Nagel).

DNA was subjected to quantitative PCR (qPCR) using KOD SYBR qPCR Mix (TOYOBO) in the StepOnePlus real-time PCR system (Thermo Fisher Scientific) (1 μL of DNA per 10 μL reaction in duplicate). Primer sets used for qPCR are listed in Table S1. The qPCR program was 95°C for 2 min (1 cycle), 95°C for 10 s, and 60°C 15 s (40 cycles), and 60 to 95°C for a dissociation curve analysis. When measuring levels of VZV DNA relative to cellular DNA using quantitative PCR, data are expressed as copies of VZV ORF10 DNA compared to copies of cellular CD24 DNA and defined as $2^{-(\text{Ct-value VZV ORF10} - \text{Ct-value CD24})}$. VZV DNA copy numbers in cell-free viruses were calculated by quantitative PCR based on a standard curve using the pOkaBAC genome (1 to 10^7 copies/reaction) and VZV ORF10 primers.

Whole viral genome Illumina sequencing and data analysis. Illumina sequencing data sets obtained in our previous analysis of pOka_P9 (passage 9), both as input virus and as virus collected from neuronal infection via axon terminals 14 days after infection (21), were reanalyzed together with virus

obtained at 24 h postinfection in the same experiments. Additional Illumina sequencing data sets were generated as part of the current study using pOka_R5 (input virus) and virus from neuron infection via axonal terminals at 24 h and 14 days after infection was used in the current study. Genomic DNA library construction, target enrichment, and sequencing on an Illumina MiSeq were performed as described previously (21). For analysis of the pOkaBAC genomes, sequencing libraries were generated using the NEBNext Ultra II DNA Library Prep Kit for Illumina (New England Biolabs) according to manufacturer's instructions and sequenced on an Illumina NovaSeq.

For all data sets, sequence reads were trimmed using TrimGalore (https://www.bioinformatics.babraham.ac.uk/projects/trim_galore/) [--paired --length 30 --quality 30] and competitively aligned against a genome index comprising both the VZV strain pOka genome (AB097933.1) and HG38 using bowtie2 [--no-discordant --end-to-end --no-mixed] (73). Postalignment processing was performed using SAMtools (74) and bam-readcount [-w 10 -d 1000000] (https://github.com/genome/bam-readcount) prior to variant calling using variant_caller_v1.0.py (https://github.com/DepledgeLab/vzv-2.0/tree/master/extras).

Plasmids. ORF31 was amplified by PCR of DNA from VZV pOka-infected MRC-5 cells using primers ORF31up16ecoF and ORF31xhoR (Table S1). The KOD-Plus-Ver. 2 PCR system (TOYOBO) was used for PCR, and the program was 1 cycle of 94°C for 2 min, 30 cycles of 98°C for 10 s, 60°C for 30 s, and 68°C for 1.5 min. The PCR product was digested with EcoRI and XhoI restriction enzymes and cloned into pCAGGS_MCS_puro plasmid (CAG_empty) via EcoRI and XhoI sites. The resulting ORF31 expression plasmids were named CAG_gB699R and CAG_gB699Q, which has G and A at nt position 2096 in ORF31 gene, respectively. The ORF31 gene in the plasmids was sequenced by primers CAG1631F and CAG1853R (Table S1), which anneal upstream and downstream of the multiple cloning site of the pCAGGS_MCS_puro plasmid. This confirmed that the ORF31 sequences were identical with pOka_AB097933.1 except G at 2096 (2096G) in CAG_gB699R. CAG_gH and CAG_gL plasmids were generated as described for CAG_gB but cloned into pCAGGS_MCS plasmid using primers ORF37up23ecoF and ORF37xhoR or ORF60up21ecoF and ORF60xhoR, respectively (Table S1). The pCAGGS plasmid was kindly provided by Jun-ichi Miyazaki (Osaka University) (75).

A DNA fragment containing pOka ORF31 was amplified by PCR of DNA from VZV pOka-infected MRC-5 cells using primers ORF31up16ecoF and pOkaR60036 (Table S1). The PCR product was cloned into pCR2.1-TOPO TA vector (TOPO TA Cloning Kit; Thermo Fisher Scientific), and the sequence of ORF31 was confirmed using the primers. The fragment containing ORF31 with 2096G or 2096A was digested with EcoRI and cloned into the EcoRI site of pBlueScript II SK(-) (Agilent). The plasmids were further digested with SacI and XhoI and cloned into plasmid pST76A-SR using SacI and XhoI sites, resulting in pST76A-SR_ORF31_2096G and pST76A-SR_ORF31_2096A. The pST76A-SR shuttle plasmid was a kind gift from by Ulrich H. Koszinowski (Max von Pettenkofer Institut, Ludwig-Maximilians-Universität München) (76).

pT7EMCLuc carrying a firefly luciferase gene under the control of the T7 promoter (77) and pCAGT7 containing the T7 RNA polymerase gene under the control of the CAG promoter (78) were generous gifts from Richard Longnecker (Northwestern University). A T7 RNA polymerase expression cassette was amplified by PCR of pCAGT7 using primers CAG1631F and CAG1878R and fused with a PCR fragment of pCAGGS_MCS_puro (CAG1878F and CAG1631R) using In-Fusion HD Cloning kit according to the manufacturer's instruction (Clontech), resulting in pCAG_puro_T7pol. The KOD-Plus-Ver. 2 PCR system (TOYOBO) was used for PCR and the program was 1 cycle of 94°C for 2 min, 30 cycles of 98°C for 10 s, 60°C for 30 s, and 68°C for 3 min.

RecA-mediated BAC mutagenesis in *E. coli*, reconstitution of recombinant virus, and BAC cassette excision. DH10B *E. coli* containing the pOkaBAC (30) were transformed with plasmid pST76A-SR_ORF31_2096A and recA-mediated allelic exchange was carried out as described previously (71), resulting in pOkaBAC_ORF31_2096A. DH10B cells containing pOkaBAC_ORF31_2096A were transformed with plasmid pST76A-SR_ORF31_2096G, and pOkaBAC_ORF31_2096G was generated using the same procedure. pOkaBAC, pOkaBAC_ORF31_2096A, and pOkaBAC_ORF31_2096G were purified (Genopure Plasmid Maxi Kit; Roche Diagnostics), subjected to restriction fragment length polymorphism analysis using BamHI or EcoRI and the region used for allelic exchange was sequenced.

The purified BAC genome (1 μg) was mixed with PEImax solution (3 μL) prepared as described previously (79) and transfected to MRC-5 cells. After cytopathic effects were seen in cells expressing green fluorescent protein within the BAC cassette, cell-free virus was prepared as described above and used to infect MeWo_Cre cells to excise the BAC cassette using the Cre/loxP system, resulting in rpOka_gB699Q (from pOkaBAC_ORF31_2096A) and rpOka_gB699R (from pOkaBAC_ORF31_2096G).

Generation of the membrane protein enriched extracellular vesicles. MEPPV_gBs and MPEEV_empty were prepared as described previously (39) with some modifications. HEK-293T cells (4×10^6) were plated in 10-cm dishes in 15 mL medium 1 day before transfection. Medium was removed and replaced with 10 mL of fresh medium just prior to transfection. CAG_empty, CAG_gB699R, or CAG_gB699Q plasmids (30 μg) were mixed with PEImax solution (60 μL) in KnockoutDMEM/F-12 (250 μL per dish) and added to HEK-293T cells. At 16 h posttransfection, medium was replaced with fresh medium and cells were cultured for 2 days. Supernatants were then filtrated (0.45 μm filters) and subjected to purification through Histodenz (Sigma-Aldrich; 20% [wt/vol] in PBS) by ultracentrifugation at 100,000 $\times$ *g* for 1 h at 4°C in a P28S rotor (CPWX80; Hitachi Koki), and the pellets were diluted in KnockoutDMEM/F-12 (400 μL) and stored at −80°C until use. Protein quantity in purified MPEEVs was measured using a Qubit 4 Fluorometer and a Qubit Protein assay kit (Thermo Fisher Scientific).

Antibodies. Rabbit anti-gB polyclonal antibody, mouse anti-gB monoclonal antibody (MAb) (clone 8), mouse anti-gE MAb (clone 9), mouse anti-gH MAb (clone VgIII-3), and mouse anti-ORF62 MAb (clone 2-B) were described previously (72, 80–82). Mouse anti-α-tubulin MAb (clone B-5-1-2) and sheep anti-TGN46 antibody were obtained from Sigma-Aldrich and AbD Serotech, respectively. Alexa Fluor 488-conjugated donkey anti-mouse IgG, Alexa Fluor 594-conjugated donkey anti-rabbit IgG, and Alexa Fluor

647-conjugated donkey anti-sheep IgG (Thermo Fisher Scientific) were used as secondary antibodies for indirect immunofluorescence assays and flow cytometry. Anti-mouse IgG horseradish peroxidase (HRP)-linked sheep or anti-rabbit IgG HRP-linked donkey antibodies (GE Healthcare Bio-Sciences) were used as secondary antibodies for immunoblotting.

Immunofluorescent staining and confocal microscopy. Cells on CELLview slides (Greiner Bio-One) were fixed with 4% (vol/vol) paraformaldehyde (PFA)/PBS at room temperature for 20 min, permeabilized with 0.1% Triton X-100/4% PFA/PBS at room temperature for 20 min, and incubated with human Fc receptor blocking solution (5% FBS/PBS containing 10% of Clear Back; MBL Life Science) at room temperature for 1 h. Cells were stained with the primary antibodies diluted in 5% FBS/PBS overnight at 4°C (1:100 for anti-gB polyclonal antibody, anti-gB Mab, and anti-TGN46 antibody), washed with 0.1% Tween 20/PBS (PBS-T) for 5 min three times, stained with secondary antibodies (1:300) diluted in 5% FBS/PBS at room temperature for 1 h, washed with PBS-T for 5 min 3 times, covered with VECTASHIELD Vibrance Antifade Mounting Medium with DAPI (Vector Laboratories), and imaged by an FV1000D confocal microscopy (Olympus).

Immunoblotting. Cells were incubated in RIPA lysis buffer (0.01 M Tris-HCl [pH 7.4], 0.15 M NaCl, 1% sodium deoxycholate, 1% Nonidet P-40, and 0.1% SDS) on ice for 15 min, sonicated in a water bath for 10 min, and centrifuged at 20,000 $\times$ *g* for 10 min. Supernatant was boiled with LDS Sample Buffer (4$\times$) and Sample Reducing Agent (DTT) (10$\times$) at 100°C for 5 min (Thermo Fisher Scientific). Proteins were separated on 4 to 12% Bis-Tris Plus Gel in MES SDS Running Buffer (200 V, 25 min) and transferred onto PVDF membranes (0.2 μm) using a Mini Blot Module (20 V, 1 h) in Bolt Transfer Buffer containing 10% methanol and 0.1% Bolt Antioxidant (Thermo Fisher Scientific). The membrane was blocked in a blocking buffer (5% [wt/vol] skim milk/0.1% Tween 20/PBS) at room temperature for 1 h, stained with primary antibodies diluted in the blocking buffer (1:3,000 for anti-gB polyclonal antibody, 1:5,000 for anti-gH MAb) overnight at 4°C, washed with PBS-T for 5 min three times, stained with the secondary antibodies diluted in the blocking buffer (1:3,000) at room temperature for 1 h, and washed with PBS-T for 5 min three times and PBS briefly once. Signals were visualized by Chemi-Lumi One Super (Nacalai Tesque, Inc.) and captured using LAS4000mini (GE Healthcare Bio-Sciences). Membranes stained with anti-gB polyclonal antibody were stripped by WB Stripping Solution Strong in accordance with the manufacturer's manual (Nacalai Tesque, Inc.) and reprobed with anti-α-tubulin MAb (1:30,000).

Flow cytometry. Cells were treated with trypLE (Thermo Fisher Scientific) at 37°C for 5 min, collected in medium (DMEM+GlutaMAX-I supplemented with heat-inactivated 8% FBS), and centrifuged at 200 $\times$ *g* for 4 min. Cell pellets were fixed with 4% PFA/PBS at room temperature for 20 min, washed with 5% FBS/PBS once, and incubated with human Fc receptor blocking solution (5% FBS/PBS containing 10% of Clear Back) at room temperature for 1 h. Cells were incubated with the primary antibody (1:200 dilution in 100 μL of 5% FBS/PBS) on ice for 1 h, washed with 5% FBS/PBS once, and incubated with secondary antibody (Alexa Fluor 488-conjugated donkey anti-mouse IgG; 1:300 dilution in 50 μL of 5% FBS/PBS) on ice for 30 min. Cell surface expression of each viral protein was analyzed using a SA3800 spectrum analyzer (Sony Corporation).

Infectious focus formation and viral growth assays. Cells (1×10^5) were seeded on one well of a 12-well plate 2 days before infection and inoculated with VZV cell-free virus for 1 h at 37°C. The number of PFU of VZV in the cell-free inoculum was calculated based on titration in MRC-5 cells. After infection, the inoculum was removed, and the cells were washed with medium and cultured. For MeWo cells, the culture medium was supplemented with 3% FBS instead 8% FBS and changed every 3 days.

For the infectious focus formation assay, the cells were infected with cell-free virus (100, 10, and 1 μL) and cultured for 7 days. For the viral growth assay, cells infected with 50 PFU of cell-free virus (at a multiplicity of infection of 0.0005) were harvested at 24-h intervals and then titrated on the same cell type. Infected cells were fixed with 4% PFA/PBS, stained with anti-gE MAb (1:10 dilution in PBS) followed by anti-mouse IgG HRP-linked sheep antibody (1:6,000 dilution in PBS), and incubated with 3,3′,5,5′-tetramethylbenzidine-H peroxidase substrate (Moss, Inc.). For the infectious focus formation assay, images of foci were captured and traced, and areas were measured using ImageJ (http://rsbweb.nih.gov/ij/).

Quantitative cell-to-cell fusion assay. Effector HEK-293T cells (6×10^5 cells/well) were seeded in 12-well plates and transfected in duplicate with plasmids (total 1 μg/well; 0.25 μg for empty, gB, gH, gL, and pT7EMCLuc) and 2.5 μL of PEImax solution mixed in 50 μL of knockoutDMEM/F-12. Target ARPE-19 cells (4×10^6 cells) were transfected with pCAG_puro_T7pol (8 μg) using Nucleofector II (kit V, program X-005, Amaxa), and the cells were divided into 4 wells of 6-well plates and cultured in RPMI 1640+GlutaMAX-I supplemented with heat-inactivated 8% FBS (3 mL). At 16 h posttransfection, cells were rinsed with PBS twice, released from wells using trypLE, and resuspended in DMEM+GlutaMAX-I supplemented with heat-inactivated 8% FBS. Target MeWo_T7pol cells were rinsed with PBS once, released from wells using trypLE and resuspended in DMEM+GlutaMAX-I supplemented with heat-inactivated 8% FBS. Effector cells and target cells were then mixed at a 1:1 ratio and coincubated at 37°C for 24 or 48 h in 24-well plates. The cells were scraped, centrifuged at 300 $\times$ *g* for 4 min, and incubated in 20 μL of ONE-Glo reagent (Promega) after removal of the supernatant. Luciferase activity was measured by TriStar LB 941 Multimode Microplate Reader (Berthold Technologies).

Data availability. All sequencing data sets generated as part of this study are available via the European Nucleotide Archive under accession PRJEB53195. Sequencing data sets from our previous work (21) are available via accession PRJEB45678.

SUPPLEMENTAL MATERIAL

Supplemental material is available online only.

FIG S1, PDF file, 0.1 MB.
TABLE S1, PDF file, 0.04 MB.

ACKNOWLEDGMENTS

This work was supported by Japan Society for the Promotion of Science (JSPS KAKENHI JP17K008858), the Ministry of Education, Culture, Sports, Science and Technology (MEXT KAKENHI JP21H02741), Grant-in-Aid from the Tokyo Biochemical Research Foundation (to T.S.), and the Intramural Research Program of the National Institute of Allergy and Infectious Diseases (NIAID), National Institutes of Health (NIH) (to J.I.C.). T.S. was supported by the Japan Herpesvirus Infections Forum while at NIH. J.B. was partially funded by the University College London/University College London Hospital (UCL/UCLH) Biomedical Research Centre (BRC). A.V. received funding from the Maryland Stem Cell Research Fund and NIH, National Institute of Neurological Disorders and Stroke (R21NS107991). We acknowledge support from the MRC and BRC for the UCL/UCLH Pathogen Sequencing Pipeline.

The funders had no role in study design, data collection, and interpretation or in the decision to submit the work for publication.

We are grateful to Yasuko Mori for use of laboratory equipment. We thank Anthony Armstrong and Amitava Roy (Bioinformatics and Computational Biosciences Branch, Office of Cyber Infrastructure and Computational Biology, NIAID, NIH) for assistance with computational studies.

REFERENCES

1. Takahashi M, Otsuka T, Okuno Y, Asano Y, Yazaki T, Isomura S. 1974. Live vaccine used to prevent the spread of varicella in children in hospital. Lancet 304:1288–1290. https://doi.org/10.1016/S0140-6736(74)90144-5.
2. Marin M, Meissner HC, Seward JF. 2008. Varicella prevention in the United States: a review of successes and challenges. Pediatrics 122:e744–e751. https://doi.org/10.1542/peds.2008-0567.
3. Willis ED, Woodward M, Brown E, Popmihajlov Z, Saddier P, Annunziato PW, Halsey NA, Gershon AA. 2017. Herpes zoster vaccine live: a 10 year review of post-marketing safety experience. Vaccine 35:7231–7239. https://doi.org/10.1016/j.vaccine.2017.11.013.
4. Chaves SS, Haber P, Walton K, Wise RP, Izurieta HS, Schmid DS, Seward JF. 2008. Safety of varicella vaccine after licensure in the United States: experience from reports to the vaccine adverse event reporting system, 1995-2005. J Infect Dis 197(Suppl 2):S170–177. https://doi.org/10.1086/522161.
5. Galea SA, Sweet A, Beninger P, Steinberg SP, LaRussa PS, Gershon AA, Sharrar RG. 2008. The safety profile of varicella vaccine: a 10-year review. J Infect Dis 197(Suppl 2):S165–169. https://doi.org/10.1086/522125.
6. Goulleret N, Mauvisseau E, Essevaz-Roulet M, Quinlivan M, Breuer J. 2010. Safety profile of live varicella virus vaccine (Oka/Merck): five-year results of the European Varicella Zoster Virus Identification Program (EU VZVIP). Vaccine 28:5878–5882. https://doi.org/10.1016/j.vaccine.2010.06.056.
7. Weinmann S, Chun C, Schmid DS, Roberts M, Vandermeer M, Riedlinger K, Bialek SR, Marin M. 2013. Incidence and clinical characteristics of herpes zoster among children in the varicella vaccine era, 2005-2009. J Infect Dis 208:1859–1868. https://doi.org/10.1093/infdis/jit405.
8. Yoshikawa T, Ando Y, Nakagawa T, Gomi Y. 2016. Safety profile of the varicella vaccine (Oka vaccine strain) based on reported cases from 2005 to 2015 in Japan. Vaccine 34:4943–4947. https://doi.org/10.1016/j.vaccine.2016.08.044.
9. Alexander KE, Tong PL, Macartney K, Beresford R, Sheppeard V, Gupta M. 2018. Live zoster vaccination in an immunocompromised patient leading to death secondary to disseminated varicella zoster virus infection. Vaccine 36:3890–3893. https://doi.org/10.1016/j.vaccine.2018.05.078.
10. Lal H, Cunningham AL, Godeaux O, Chlibek R, Diez-Domingo J, Hwang S-J, Levin MJ, McElhaney JE, Poder A, Puig-Barberà J, Vesikari T, Watanabe D, Weckx L, Zahaf T, Heineman TC, Group Z-50 S. 2015. Efficacy of an adjuvanted herpes zoster subunit vaccine in older adults. N Engl J Med 372:2087–2096. https://doi.org/10.1056/NEJMoa1501184.
11. Cunningham AL, Lal H, Kovac M, Chlibek R, Hwang S-J, Díez-Domingo J, Godeaux O, Levin MJ, McElhaney JE, Puig-Barberà J, Abeele CV, Vesikari T, Watanabe D, Zahaf T, Ahonen A, Athan E, Barba-Gomez JF, Campora L, de Looze F, Downey HJ, Ghesquiere W, Gorfinkel I, Korhonen T, Leung E, McNeil SA, Oostvogels L, Rombo L, Smetana J, Weckx L, Yeo W, Heineman TC, ZOE-70 Study Group. 2016. Efficacy of the herpes zoster subunit vaccine in adults 70 years of age or older. N Engl J Med 375:1019–1032. https://doi.org/10.1056/NEJMoa1603800.
12. Jacquet A, Haumont M, Massaer M, Garcia L, Mazzu P, Daminet V, Grégoire D, Jacobs P, Bollen A. 2002. Immunogenicity of a recombinant varicella-zoster virus gE–IE63 fusion protein, a putative vaccine candidate against primary infection and zoster reactivation. Vaccine 20:1593–1602. https://doi.org/10.1016/S0264-410X(01)00486-8.
13. Dendouga N, Fochesato M, Lockman L, Mossman S, Giannini SL. 2012. Cell-mediated immune responses to a varicella-zoster virus glycoprotein E vaccine using both a TLR agonist and QS21 in mice. Vaccine 30:3126–3135. https://doi.org/10.1016/j.vaccine.2012.01.088.
14. Redman RL, Nader S, Zerboni L, Liu C, Wong RM, Brown BW, Arvin AM. 1997. Early reconstitution of immunity and decreased severity of herpes zoster in bone marrow transplant recipients immunized with inactivated varicella vaccine. J Infect Dis 176:578–585. https://doi.org/10.1086/514077.
15. Hata A, Asanuma H, Rinki M, Sharp M, Wong RM, Blume K, Arvin AM. 2002. Use of an inactivated varicella vaccine in recipients of hematopoietic-cell transplants. N Engl J Med 347:26–34. https://doi.org/10.1056/NEJMoa013441.
16. Levin MJ, Oxman MN, Zhang JH, Johnson GR, Stanley H, Hayward AR, Caulfield MJ, Irwin MR, Smith JG, Clair J, Chan ISF, Williams H, Harbecke R, Marchese R, Straus SE, Gershon A, Weinberg A, Investigators VACSPSPS. 2008. Varicella-zoster virus-specific immune responses in elderly recipients of a herpes zoster vaccine. J Infect Dis 197:825–835. https://doi.org/10.1086/528696.
17. Sadaoka T, Mori Y. 2018. Vaccine development for varicella-zoster virus. Adv Exp Med Biol 1045:123–142. https://doi.org/10.1007/978-981-10-7230-7_7.
18. Gomi Y, Sunamachi H, Mori Y, Nagaike K, Takahashi M, Yamanishi K. 2002. Comparison of the complete DNA sequences of the Oka varicella vaccine and its parental virus. J Virol 76:11447–11459. https://doi.org/10.1128/JVI.76.22.11447-11459.2002.
19. Depledge DP, Yamanishi K, Gomi Y, Gershon AA, Breuer J. 2016. Deep sequencing of distinct preparations of the live attenuated varicella-zoster virus vaccine reveals a conserved core of attenuating single-nucleotide polymorphisms. J Virol 90:8698–8704. https://doi.org/10.1128/JVI.00998-16.
20. Depledge DP, Kundu S, Jensen NJ, Gray ER, Jones M, Steinberg S, Gershon A, Kinchington PR, Schmid DS, Balloux F, Nichols RA, Breuer J. 2014. Deep sequencing of viral genomes provides insight into the evolution and pathogenesis of varicella zoster virus and its vaccine in humans. Mol Biol Evol 31:397–409. https://doi.org/10.1093/molbev/mst210.

21. Sadaoka T, Depledge DP, Rajbhandari L, Venkatesan A, Breuer J, Cohen JI. 2016. In vitro system using human neurons demonstrates that varicella-zoster vaccine virus is impaired for reactivation, but not latency. Proc Natl Acad Sci U S A 113:E2403–E2412. https://doi.org/10.1073/pnas.1522575113.
22. Kim JI, Jung GS, Kim YY, Ji GY, Kim HS, Wang WD, Park HS, Park SY, Kim GH, Kwon SN, Lee KM, Ahn JH, Yoon Y, Lee CH. 2011. Sequencing and characterization of Varicella-Zoster virus vaccine strain SuduVax. Virol J 8:547. https://doi.org/10.1186/1743-422X-8-547.
23. Peters GA, Tyler SD, Carpenter JE, Jackson W, Mori Y, Arvin AM, Grose C. 2012. The Attenuated genotype of varicella-zoster virus includes an ORF0 transitional stop codon mutation. J Virol 86:10695–10703. https://doi.org/10.1128/JVI.01067-12.
24. Zerboni L, Hinchliffe S, Sommer MH, Ito H, Besser J, Stamatis S, Cheng J, Distefano D, Kraiouchkine N, Shaw A, Arvin AM. 2005. Analysis of varicella zoster virus attenuation by evaluation of chimeric parent Oka/vaccine Oka recombinant viruses in skin xenografts in the SCIDhu mouse model. Virology 332:337–346. https://doi.org/10.1016/j.virol.2004.10.047.
25. Koshizuka T, Ota M, Yamanishi K, Mori Y. 2010. Characterization of varicella-zoster virus-encoded ORF0 gene—comparison of parental and vaccine strains. Virology 405:280–288. https://doi.org/10.1016/j.virol.2010.06.016.
26. Zell R, Taudien S, Pfaff F, Wutzler P, Platzer M, Sauerbrei A. 2012. Sequencing of 21 varicella-zoster virus genomes reveals two novel genotypes and evidence of recombination. J Virol 86:1608–1622. https://doi.org/10.1128/JVI.06233-11.
27. Mocarski ES, Jr. 2007. In Arvin AM, Campadelli-Fiume G, Mocarski ES, Moore PS, Roizman B, Whitley R, Yamanishi K (eds). Comparative analysis of herpesvirus-common proteins. Human herpesviruses: biology, therapy, and immunoprophylaxis. Cambridge University Press, Cambridge, UK.
28. Oliver SL, Xing Y, Chen D-H, Roh SH, Pintilie GD, Bushnell DA, Sommer MH, Yang E, Carfi A, Chiu W, Arvin AM. 2020. A glycoprotein B-neutralizing antibody structure at 2.8 Å uncovers a critical domain for herpesvirus fusion initiation. Nat Commun 11:4141. https://doi.org/10.1038/s41467-020-17911-0.
29. Heldwein EE, Lou H, Bender FC, Cohen GH, Eisenberg RJ, Harrison SC. 2006. Crystal structure of glycoprotein b from herpes simplex virus 1. Science 313:217–220. https://doi.org/10.1126/science.1126548.
30. Nagaike K, Mori Y, Gomi Y, Yoshii H, Takahashi M, Wagner M, Koszinowski U, Yamanishi K. 2004. Cloning of the varicella-zoster virus genome as an infectious bacterial artificial chromosome in Escherichia coli. Vaccine 22:4069–4074. https://doi.org/10.1016/j.vaccine.2004.03.062.
31. Markus A, Lebenthal-Loinger I, Yang IH, Kinchington PR, Goldstein RS. 2015. An in vitro model of latency and reactivation of varicella zoster virus in human stem cell-derived neurons. PLoS Pathog 11:e1004885. https://doi.org/10.1371/journal.ppat.1004885.
32. Sadaoka T, Schwartz CL, Rajbhandari L, Venkatesan A, Cohen JI. 2018. Human embryonic stem cell-derived neurons are highly permissive for varicella-zoster virus lytic infection. J Virol 92:e01108-17. https://doi.org/10.1128/JVI.01108-17.
33. Grigoryan S, Yee MB, Glick Y, Gerber D, Kepten E, Garini Y, Yang IH, Kinchington PR, Goldstein RS. 2015. Direct transfer of viral and cellular proteins from varicella-zoster virus-infected non-neuronal cells to human axons. PLoS One 10:e0126081. https://doi.org/10.1371/journal.pone.0126081.
34. Ouwendijk WJD, Depledge DP, Rajbhandari L, Rovis TL, Jonjic S, Breuer J, Venkatesan A, Verjans GMGM, Sadaoka T. 2020. Varicella-zoster virus VLT-ORF63 fusion transcript induces broad viral gene expression during reactivation from neuronal latency. Nat Commun 11:6324. https://doi.org/10.1038/s41467-020-20031-4.
35. Oliver SL, Sommer M, Zerboni L, Rajamani J, Grose C, Arvin AM. 2009. Mutagenesis of varicella-zoster virus glycoprotein B: putative fusion loop residues are essential for viral replication, and the furin cleavage motif contributes to pathogenesis in skin tissue in vivo. J Virol 83:7495–7506. https://doi.org/10.1128/JVI.00400-09.
36. Soong W, Schultz JC, Patera AC, Sommer MH, Cohen JI. 2000. Infection of human T lymphocytes with varicella-zoster virus: an analysis with viral mutants and clinical isolates. J Virol 74:1864–1870. https://doi.org/10.1128/JVI.74.4.1864-1870.2000.
37. Oliver SL, Brady JJ, Sommer MH, Reichelt M, Sung P, Blau HM, Arvin AM. 2013. An immunoreceptor tyrosine-based inhibition motif in varicella-zoster virus glycoprotein B regulates cell fusion and skin pathogenesis. Proc Natl Acad Sci U S A 110:1911–1916. https://doi.org/10.1073/pnas.1216985110.
38. Suenaga T, Satoh T, Somboonthum P, Kawaguchi Y, Mori Y, Arase H. 2010. Myelin-associated glycoprotein mediates membrane fusion and entry of neurotropic herpesviruses. Proc Natl Acad Sci U S A 107:866–871. https://doi.org/10.1073/pnas.0913351107.
39. Zeev-Ben-Mordehai T, Vasishtan D, Siebert CA, Whittle C, Grünewald K. 2014. Extracellular vesicles: a platform for the structure determination of membrane proteins by cryo-EM. Structure 22:1687–1692. https://doi.org/10.1016/j.str.2014.09.005.
40. Zeev-Ben-Mordehai T, Vasishtan D, Durán AH, Vollmer B, White P, Pandurangan AP, Siebert CA, Topf M, Grünewald K. 2016. Two distinct trimeric conformations of natively membrane-anchored full-length herpes simplex virus 1 glycoprotein B. Proc Natl Acad Sci U S A 113:4176–4181. https://doi.org/10.1073/pnas.1523234113.
41. Tommasi C, Breuer J. 2022. The biology of varicella-zoster virus replication in the skin. Viruses 14:982. https://doi.org/10.3390/v14050982.
42. Moffat JF, Zerboni L, Kinchington PR, Grose C, Kaneshima H, Arvin AM. 1998. Attenuation of the vaccine oka strain of varicella-zoster virus and role of glycoprotein C in alphaherpesvirus virulence demonstrated in the SCID-hu mouse. J Virol 72:965–974. https://doi.org/10.1128/JVI.72.2.965-974.1998.
43. Cole NL, Grose C. 2003. Membrane fusion mediated by herpesvirus glycoproteins: the paradigm of varicella-zoster virus. Rev Med Virol 13:207–222. https://doi.org/10.1002/rmv.377.
44. Zhang Z, Selariu A, Warden C, Huang G, Huang Y, Zaccheus O, Cheng T, Xia N, Zhu H. 2010. Genome-wide mutagenesis reveals that ORF7 is a novel VZV skin-tropic factor. PLoS Pathog 6:e1000971. https://doi.org/10.1371/journal.ppat.1000971.
45. Zmasek CM, Knipe DM, Pellett PE, Scheuermann RH. 2019. Classification of human Herpesviridae proteins using Domain-architecture Aware Inference of Orthologs (DAIO). Virology 529:29–42. https://doi.org/10.1016/j.virol.2019.01.005.
46. Thiele S, Borschewski A, Küchler J, Bieberbach M, Voigt S, Ehlers B. 2011. Molecular analysis of varicella vaccines and varicella-zoster virus from vaccine-related skin lesions. Clin Vaccine Immunol 18:1058–1066. https://doi.org/10.1128/CVI.05021-11.
47. Wu Q, Rivailler P, Xu S, Xu W. 2019. Comparison of the whole-genome sequence of an oka varicella vaccine from china with other oka vaccine strains reveals sites putatively critical for vaccine efficacy. J Virol 93:1759. https://doi.org/10.1128/JVI.02281-18.
48. Cohen JI, Seidel KE. 1993. Generation of varicella-zoster virus (VZV) and viral mutants from cosmid DNAs: VZV thymidylate synthetase is not essential for replication in vitro. Proc Natl Acad Sci U S A 90:7376–7380. https://doi.org/10.1073/pnas.90.15.7376.
49. Moffat JF, Stein MD, Kaneshima H, Arvin AM. 1995. Tropism of varicella-zoster virus for human CD4+ and CD8+ T lymphocytes and epidermal cells in SCID-hu mice. J Virol 69:5236–5242. https://doi.org/10.1128/jvi.69.9.5236-5242.1995.
50. Jeon JS, Won YH, Kim IK, Ahn JH, Shin OS, Kim JH, Lee CH. 2016. Analysis of single nucleotide polymorphism among Varicella-Zoster Virus and identification of vaccine-specific sites. Virology 496:277–286. https://doi.org/10.1016/j.virol.2016.06.017.
51. Backovic M, Longnecker R, Jardetzky TS. 2009. Structure of a trimeric variant of the Epstein–Barr virus glycoprotein B. Proc Natl Acad Sci U S A 106:2880–2885. https://doi.org/10.1073/pnas.0810530106.
52. Cooper RS, Georgieva ER, Borbat PP, Freed JH, Heldwein EE. 2018. Structural basis for membrane anchoring and fusion regulation of the herpes simplex virus fusogen gB. Nat Struct Mol Biol 25:416–424. https://doi.org/10.1038/s41594-018-0060-6.
53. Chandramouli S, Ciferri C, Nikitin PA, Caló S, Gerrein R, Balabanis K, Monroe J, Hebner C, Lilja AE, Settembre EC, Carfi A. 2015. Structure of HCMV glycoprotein B in the postfusion conformation bound to a neutralizing human antibody. Nat Commun 6:8176. https://doi.org/10.1038/ncomms9176.
54. Burke HG, Heldwein EE. 2015. Crystal structure of the human cytomegalovirus glycoprotein B. PLoS Pathog 11:e1005227. https://doi.org/10.1371/journal.ppat.1005227.
55. Connolly SA, Jardetzky TS, Longnecker R. 2021. The structural basis of herpesvirus entry. Nat Rev Microbiol 19:110–112. https://doi.org/10.1038/s41579-020-00448-w.
56. Fontana J, Atanasiu D, Saw WT, Gallagher JR, Cox RG, Whitbeck JC, Brown LM, Eisenberg RJ, Cohen GH. 2017. The fusion loops of the initial prefusion conformation of herpes simplex virus 1 fusion protein point toward the membrane. mBio 8:e01268-17. https://doi.org/10.1128/mBio.01268-17.
57. Vollmer B, Pražák V, Vasishtan D, Jefferys EE, Hernandez-Duran A, Vallbracht M, Klupp BG, Mettenleiter TC, Backovic M, Rey FA, Topf M, Grünewald K. 2020. The prefusion structure of herpes simplex virus glycoprotein B. Sci Adv 6:eabc1726. https://doi.org/10.1126/sciadv.abc1726.

58. Melikyan GB, Markosyan RM, Hemmati H, Delmedico MK, Lambert DM, Cohen FS. 2000. Evidence that the transition of HIV-1 Gp41 into a six-helix bundle, not the bundle configuration, induces membrane fusion. J Cell Biol 151:413–424. https://doi.org/10.1083/jcb.151.2.413.
59. Russell CJ, Jardetzky TS, Lamb RA. 2001. Membrane fusion machines of paramyxoviruses: capture of intermediates of fusion. EMBO J 20:4024–4034. https://doi.org/10.1093/emboj/20.15.4024.
60. Lamb RA, Jardetzky TS. 2007. Structural basis of viral invasion: lessons from paramyxovirus F. Curr Opin Struct Biol 17:427–436. https://doi.org/10.1016/j.sbi.2007.08.016.
61. Connolly SA, Longnecker R. 2012. Residues within the C-terminal arm of the herpes simplex virus 1 glycoprotein B Ectodomain contribute to its refolding during the fusion step of virus entry. J Virol 86:6386–6393. https://doi.org/10.1128/JVI.00104-12.
62. Lopper M, Compton T. 2004. Coiled-coil domains in glycoproteins B and H are involved in human cytomegalovirus membrane fusion. J Virol 78:8333–8341. https://doi.org/10.1128/JVI.78.15.8333-8341.2004.
63. Chan DC, Kim PS. 1998. HIV entry and its inhibition. Cell 93:681–684. https://doi.org/10.1016/S0092-8674(00)81430-0.
64. Bauer D, Alt M, Dirks M, Buch A, Heilingloh CS, Dittmer U, Giebel B, Görgens A, Palapys V, Kasper M, Eis-Hübinger AM, Sodeik B, Heiligenhaus A, Roggendorf M, Krawczyk A. 2017. A Therapeutic antiviral antibody inhibits the anterograde directed neuron-to-cell spread of herpes simplex virus and protects against ocular disease. Front Microbiol 8:2115. https://doi.org/10.3389/fmicb.2017.02115.
65. Jones M, Dry IR, Frampton D, Singh M, Kanda RK, Yee MB, Kellam P, Hollinshead M, Kinchington PR, O'Toole EA, Breuer J. 2014. RNA-seq analysis of host and viral gene expression highlights interaction between varicella zoster virus and keratinocyte differentiation. PLoS Pathog 10:e1003896. https://doi.org/10.1371/journal.ppat.1003896.
66. Tommasi C, Rogerson C, Depledge DP, Jones M, Naeem AS, Venturini C, Frampton D, Tutill HJ, Way B, Breuer J, O'Shaughnessy RFL. 2020. Kallikrein-mediated cytokeratin 10 degradation is required for VZV propagation in skin. J Invest Dermatol 140:774–784.e11. https://doi.org/10.1016/j.jid.2019.08.448.
67. Lloyd MG, Smith NA, Tighe M, Travis KL, Liu D, Upadhyaya PK, Kinchington PR, Chan GC, Moffat JF. 2020. A novel human skin tissue model to study varicella-zoster virus and human cytomegalovirus. J Virol 94:e01082-20. https://doi.org/10.1128/JVI.01082-20.
68. Taylor SL, Moffat JF. 2005. Replication of varicella-zoster virus in human skin organ culture. J Virol 79:11501–11506. https://doi.org/10.1128/JVI.79.17.11501-11506.2005.
69. Garza ZCF, Lenz M, Liebmann J, Ertaylan G, Born M, Arts ICW, Hilbers PAJ, van Riel NAW. 2019. Characterization of disease-specific cellular abundance profiles of chronic inflammatory skin conditions from deconvolution of biopsy samples. BMC Med Genomics 12:121. https://doi.org/10.1186/s12920-019-0567-7.
70. Tegenge MA, Rajbhandari L, Shrestha S, Mithal A, Hosmane S, Venkatesan A. 2014. Curcumin protects axons from degeneration in the setting of local neuroinflammation. Exp Neurol 253:102–110. https://doi.org/10.1016/j.expneurol.2013.12.016.
71. Sadaoka T, Yanagi T, Yamanishi K, Mori Y. 2010. Characterization of the varicella-zoster virus ORF50 gene, which encodes glycoprotein M. J Virol 84:3488–3502. https://doi.org/10.1128/JVI.01838-09.
72. Sadaoka T, Serada S, Kato J, Hayashi M, Gomi Y, Naka T, Yamanishi K, Mori Y. 2014. Varicella-zoster virus ORF49 functions in the efficient production of progeny virus through its interaction with essential tegument protein ORF44. J Virol 88:188–201. https://doi.org/10.1128/JVI.02245-13.
73. Langmead B, Salzberg SL. 2012. Fast gapped-read alignment with Bowtie 2. Nat Methods 9:357–359. https://doi.org/10.1038/nmeth.1923.
74. Li H, Handsaker B, Wysoker A, Fennell T, Ruan J, Homer N, Marth G, Abecasis G, Durbin R, Subgroup 1000 Genome Project Data Processing. 2009. The Sequence Alignment/Map format and SAMtools. Bioinformatics 25:2078–2079. https://doi.org/10.1093/bioinformatics/btp352.
75. Hitoshi N, Ken-ichi Y, Jun-ichi M. 1991. Efficient selection for high-expression transfectants with a novel eukaryotic vector. Gene 108:193–199. https://doi.org/10.1016/0378-1119(91)90434-D.
76. Hobom U, Brune W, Messerle M, Hahn G, Koszinowski UH. 2000. Fast screening procedures for random transposon libraries of cloned herpesvirus genomes: mutational analysis of human cytomegalovirus envelope glycoprotein genes. J Virol 74:7720–7729. https://doi.org/10.1128/JVI.74.17.7720-7729.2000.
77. Aoki Y, Aizaki H, Shimoike T, Tani H, Ishii K, Saito I, Matsuura Y, Miyamura T. 1998. A human liver cell line exhibits efficient translation of HCV RNAs produced by a recombinant adenovirus expressing T7 RNA polymerase. Virology 250:140–150. https://doi.org/10.1006/viro.1998.9361.
78. Okuma K, Nakamura M, Nakano S, Niho Y, Matsuura Y. 1999. Host range of human T-cell leukemia virus type i analyzed by a cell fusion-dependent reporter gene activation assay. Virology 254:235–244. https://doi.org/10.1006/viro.1998.9530.
79. Depledge DP, Ouwendijk WJD, Sadaoka T, Braspenning SE, Mori Y, Cohrs RJ, Verjans GMGM, Breuer J. 2018. A spliced latency-associated VZV transcript maps antisense to the viral transactivator gene 61. Nat Commun 9:1167. https://doi.org/10.1038/s41467-018-03569-2.
80. Okuno T, Yamanishi K, Shiraki K, Takahashi M. 1983. Synthesis and processing of glycoproteins of Varicella-Zoster virus (VZV) as studied with monoclonal antibodies to VZV antigens. Virology 129:357–368. https://doi.org/10.1016/0042-6822(83)90175-7.
81. Sadaoka T, Yoshii H, Imazawa T, Yamanishi K, Mori Y. 2007. Deletion in open reading frame 49 of varicella-zoster virus reduces virus growth in human malignant melanoma cells but not in human embryonic fibroblasts. J Virol 81:12654–12665. https://doi.org/10.1128/JVI.01183-07.
82. Hama Y, Shiraki K, Yoshida Y, Maruyama A, Yasuda M, Tsuda M, Honda M, Takahashi M, Higuchi H, Takasaki I, Daikoku T, Tsumoto T. 2010. Antibody to varicella-zoster virus immediate-early protein 62 augments allodynia in zoster via brain-derived neurotrophic factor. J Virol 84:1616–1624. https://doi.org/10.1128/JVI.02061-09.